Research paper

A modified Gibson-Ashby model for functionally graded lattice structures

Seyed Kamal Jalali [a], Mohammad Javad Beigrezaee [a], Diego Misseroni [b], Nicola Maria Pugno [a,c,*]

[a] *Laboratory for Bioinspired, Bionic, Nano, MetaMaterials and Mechanics, Department of Civil, Environmental and Mechanical Engineering, University of Trento, Italy*
[b] *Laboratory for the Design of Reconfigurable Metamaterials & Structures, Department of Civil, Environmental and Mechanical Engineering, University of Trento, Italy*
[c] *School of Engineering and Materials Science, Queen Mary University of London, Mile End Road, London E1 4NS, UK*

A R T I C L E   I N F O

A B S T R A C T

The current paper extends the classic Gibson-Ashby model of cellular solids for repetitive graded lattices. Three well-known porous unit cells, i.e., simple cubic (SC), body-centered cubic (BCC), and their combination (BCC⁺), are considered and the corresponding graded lattices are geometrically defined by functional variation in the diameters of the ligaments based on a power law. The analytical expressions for the relative elastic modulus of the cells, which vary along the graded direction, are provided by structural analysis of the representative beam framework containing tapered beams using the Euler–Bernoulli theory. After that, continuous approximation functions for variation of the relative density and the relative elastic modulus are presented by curve fitting over the analytical expressions along the graded direction. Then, the graded lattices are considered to be fully homogenized and as a homogeneous media, the exact expressions for the effective relative density and the effective relative modulus are presented. The modified version of the Gibson-Ashby model is proposed to relate the effective relative modulus to the effective relative density by introducing a correction factor to the classic model. It is shown that the classic Gibson-Ashby model with the coefficients fitted on uniform lattices, is not accurate for relating the effective properties of the graded lattices. The proposed model, presented as an analytical expression with fitting parameters and a correction factor, serves as a useful guideline for designing optimized functionally graded lattice structures, accommodating a wide range of geometric variations.

1. Introduction

Thanks to the recent technological advances in manufacturing methods, material scientists and designers have encountered a wide variety of novel material selections in conjunction with the possibility of producing complex geometries to accurately match the desired properties according to demanded applications. Among them, the idea of Functionally Graded (FG) change in material properties is one of the great choices due to its exceptional potential in a vast of industrial applications such as automotive (Saleh and Ahmed, 2020; Ram et al., 2017), aerospace (Popoola et al., 2016; Kumar et al., 2013), biomedical (Pompe et al., 2003; Gorgin Karaji et al., 2020), etc. Saleh et al. (2020), Parihar et al. (2018) and Mahmoud and Elbestawi (2017). In addition to the conventional composite FG materials where the functional change is only imposed by graded variation in the volume fraction of components, new additive manufacturing methods (Mora et al., 2022) suggest fabrication of advanced cellular solids (Gibson and Ashby, 2014) as lattice structures with complex graded structural architectures by functional variation in the geometrical parameters of

the cells. Not only the distribution of the type and the size of unit cells within the lattice structure can be varied in different directions but also each of the unit cells can have graded changes in the thickness of ligaments that affect the whole structural performance. Therefore, this class of porous materials possesses a remarkable perspective to replace conventional materials in many industrial applications, and hence the investigation of their properties is of particular importance (Reddy et al., 2020). They are also of interest in the field of metamaterial science (Janbaz et al., 2018; Fleck et al., 2010; van Manen et al., 2021).

From the analytical point of view, the mechanical properties of a porous cellular solid can be evaluated by common analytical structural theories derived from various geometric microstructure models (Menges and Knipschild, 1975; Gibson and Ashby, 1982; Christensen, 1986; Roberts and Garboczi, 2001). One of the most applied formulas, which is widely implemented for the open- and closed-cell foams and structures, is the power law (Maconachie et al., 2019), introduced by Gibson and Ashby (1982, 2014). This model relates the fundamental mechanical properties of lattice structure to its density,

---

* Corresponding author.
  E-mail address: nicola.pugno@unitn.it (N.M. Pugno).

defining the relative properties of the lattice as the ratio of its properties to the bulk counterpart. The Gibson-Ashby model has two constants, one of which is the power of the relative density (usually denoted by n) and the second one is the multiplier (usually denoted by C). For many cases, these two constants should be fitted with the existing data for accurate results while for simplicity, they are set for some general lattice structures as a unique value. For instance, for an open-cell foam, n is usually set to 2 and C is equal to 1 for evaluating the stiffness modulus. Although some literature (McKown et al., 2008; Zargarian et al., 2019) reported that these values for the Gibson-Ashby theory can predict the mechanical behavior with good accuracy, some other researchers (Zhang et al., 2018; Zadpoor, 2019; Yakout et al., 2019) showed that these constants should be modified according to the material and the fabrication procedure from which the cellular solid is made (Goodall, 2013).

The other reason why the Gibson-Ashby model should be fitted case by case is that different architectures for each of the unit cells of lattice structures significantly affect the mechanical response under loading. Accordingly, the mechanical properties of lattice structures have been analytically investigated by recent studies due to the advances in the additive manufacturing method, which allows the production of different types of complex unit cells. Zadpoor and Hedayati (2016). Hedayati et al. (2016b) derived an analytical solution for evaluating the mechanical properties of the porous structure made of truncated cube unit cells. Besides, they developed a finite element (FE) model and compared the results with the analytical ones. Elastic modulus and Poisson's ratio of a lattice structure with the body-centered cuboid unit cell have been analytically evaluated by Ptochos and Labeas (2012). While the well-known unit cell called body-centered cubic (BCC) has equal dimensions in all directions, the body-centered cuboid, on the other hand, has unequal dimensions in three directions. Both Timoshenko and Euler–Bernoulli's beam theories were applied to analyze the structure under complex loading conditions. Finally, they claimed that their approach is a cost-efficient method for evaluating the mechanical behavior of the lattice structure made of BCC or body-centered cuboid. Classical beam theory had been applied (Ushijima et al., 2011) for evaluating the initial specific stiffness of a BCC lattice structure. The results showed that the aspect ratio of the ligaments directly affects the accuracy of the results.

All the mentioned studies were on finding the properties of uniform lattice structures with constant geometrical and material properties of the unit cell, benefiting the Gibson-Ashby model for prediction. In parallel, some other researchers in the field of structural analysis tried to extend these formulations for uniform lattices to functionally graded porous (FGP) structural members, i.e., beams, plates, panels, shells, etc., where the porosity varies continuously within the member mostly in the direction of thickness. For this purpose, they assumed the same Gibson-Ashby model with the same parameters, mostly $n = 2$ and $C = 1$ fitted for uniform open-cell lattices, in order to define the function of variation in mechanical properties for FGP structural members and found their mechanical response under different load conditions (Jalali et al., 2022; Wu et al., 2020). By use of the pseudo-spectral method, Jalali and Heshmati (Heshmati and Jalali, 2019) numerically computed the governing equations for free vibration of the FGP circular plates where the porosity gradually changes along the radial direction and the effect of different porosity distributions alongside different boundary conditions were presented. In another study (Jalali and Heshmati, 2020), they investigated the effect of tapering on the FGP circular and annular plates having variable properties along the radial direction, and the potential of thickness variation profile for optimizing the frequency response was examined. Jalali et al. (2021), probed the possibility of extending the closed-form solutions of homogeneous plates under different loading conditions to the FGP ones. Many case studies were performed and they claimed that it was not necessary to resolve the governing equation of the plate theories for the plates with FGP along the thickness since the available exact solutions in the literature on homogeneous plates could be used by substituting the corresponding out-of-plane and in-plane rigidity and moments of inertia of FGP plate. Therefore, they presented the exact expression of these rigidities and moments of inertia for 12 different porosity distributions by integrating them across the thickness. In a recent study (Jalali et al., 2022), a misunderstanding was reported regarding the relationship between the mechanical properties of FGP structures and density. The study established a local (point-by-point) version of the Gibson-Ashby model. They showed that this misunderstanding which is observed in a large number of publications in the literature led to an undeniable error in predicting both the statics and dynamics mechanical response of the FGP structure.

According to Bai et al. (2020), FGP materials can be divided into four categories including changing the material properties, changing the unit cell type, scaling the unit cell, and changing the diameter of the unit cell ligaments which the latest one has the most structural integrity compared to the other methods. The results showed that their new configuration, which was based on BCC unit cells, had a great capability of absorbing energy under large strain and efficient support under small strain. They also claimed that the Gibson-Ashby theory could accurately predict the mechanical properties of their lattice configuration. In continuing this work, Rodrigo et al. (2021) studied the deformation pattern of an FG lattice structure based on BCC unit cells and compared it with the uniform one. Maskery et al. (2017) considered the standard BCC unit cell and its reinforced version by adding struts in the direction of applied load (named BCC_z) in order to compare the collapse deformation process from the video recording with the properties of the stress–strain diagram. Choy et al. (2017) experimentally studied the energy absorption of FG cubic and honeycomb lattice structures with graded changes in the diameter of ligaments fabricated by selective laser melting (SLM), with Ti-6Al-4V as the building material and showed that the energy absorption capability is significantly affected by the direction of loading. In other two related studies, Al-Saedi et al. (2018) and Al-Saedi and Masood (2018) described energy absorption capacity and mechanical properties of uniform and FG lattice structure using the combination of BCC and face-centered cubic unit cell, called F2BCC, and the general conclusion is similar to those reported in Maskery et al. (2017) and Choy et al. (2017) saying that the uniform lattice structure had a shear failure mode of 45° at its peak of compression stress. However, FG lattice structures obviously collapsed layer by layer consecutively from the lowest to the highest density layer. In addition, the FG lattice structure with F2BCC unit cells showed higher energy absorption despite the earlier beginning of densification strain compared to the uniform one. They also announced that the cumulative energy absorption per unit volume as a function of strain was increased exponentially for FG lattice structure, while it was bilinear for uniform one. Mahbod and Asgari (2019) introduced a new configuration for the unit cell of FG structures by a step-wise change in the diameters of ligaments (layer by layer of cells along the graded direction) and characterized the elastic and plastic properties via an analytical model which was previously provided in Hedayati et al. (2016b,a). While a good correlation between analytical, numerical, and experimental data was obtained, they claimed that the new unit cell could be compatible with various applications because of the versatile design methodology for manufacturing the desired material properties. In one of the most recent studies, a new unit cell, containing 16 connection nodes and 32 inclined struts, was introduced by Gharehbaghi et al. (2022) and the elasticity modulus in two directions along with Poisson's ratio were assessed via the equations of Euler–Bernoulli beam theory and the effect of step changes in the diameter of struts as an FG graded lattice is investigated. They also analyzed the layer-wised FG structure with three overall porosity and the numerical and experimental results revealed a good correlation with the analytical ones.

To the best knowledge of the authors, there is no exact analytical solution for evaluating the relative density and the relative stiffness

modulus of FG lattice structures. Therefore, the current paper aims to parameterize the variation in the architecture of these nonuniform lattices with a variable diameter of ligaments for different types of common unit cells in order to find the analytical expression for evaluating the relative density and stiffness modulus. Among the huge library of unit cells with exceptional mechanical properties, Cao et al. (2018, 2020, 2021), three well-known unit cells, i.e., simple cube, body-centered cubic, and their combination are selected. Next, from a fully homogenized point of view, the closed-form formulas for the effective density and effective modulus of FG lattices are derived. Besides, approximation functions for the estimation of the relative density and the relative elastic modulus along the graded direction are presented by the use of curve fitting over analytical solutions. Finally, a modified Gibson-Ashby model with a correction factor is introduced which can relate accurately the effective relative stiffness modulus to the effective relative density. The presented calibrated correction factor covers a wide range of variations in the diameter of the ligament for three types of considered unit cells.

2. Methodology

2.1. The geometric definition of graded lattices

Consider a cubic unit cell of a length side l and a main diagonal $\sqrt{3}l$ which can construct three well-known lattices i.e., simple cubic (SC) where only the sides of the cube are kept, the body-centered cubic (BCC) where only the main diagonals are kept, and their combination (BCC$^+$). One should note that in a 3D repetition, every side is shared between four neighboring cells, while the diagonals belong exclusively to the cell. A lattice structure is built up by placing the ligaments of nominal diameter d on the sides and/or the diagonals. It is useful to define the dimensionless ratio of a ligament, $R = d/l$, for the purpose of generality.

A graded lattice structure can be achieved in three ways: First, a gradual change in the properties of the bulk material having a uniform lattice geometry, second, a gradual change in the lattice constant fixing the bulk material and the diameter of ligaments, and third, a gradual change in the diameter of ligaments keeping constant the bulk material and the lattice constant. Here, the last one is selected because the first one faces the difficulties of multi-material fabrication, and the second, although is identical to the idea of gradual change in the pore size for an irregular 3D foam, presents difficulties when it is applied to a regular lattice. Fig. 1 illustrates the schematic of the functionally graded lattice under study. It is assumed that the dimensionless diameter of ligaments, R, varies along x axis, through N cells with the total length of $L = Nl$ from R_0 at $x = 0$ to R_N at $x = L$. Because of the discontinuous nature of lattice, the variation function should be defined in a clear way for all the ligaments which are categorized into three groups: those lying on the sides of cubes on the $y - z$ planes, those on the sides of the cubes parallel to the gradual direction, i.e., x, and those placed on the diagonals. The definition of the graded lattice starts with the first category, where it is assumed that the dimensionless diameter of ligaments laid on $y-z$ planes varies according to a power law as follows:

$$R_{yz}^{(j)} = R_0 + \Delta R \left(\frac{j}{N} \right)^m \tag{1}$$

where $\Delta R = R_N - R_0$ and $j = 1, 2, \ldots, N$. Then, the ligaments parallel to x axis as well as the diagonal ones are divided by N interval placed among $N+1$ groups of ligaments on $y-z$ planes. The ligaments parallel to the x axis are assumed to have a tapering variation forming conical frustums. For kth cell, $k = 1, 2, \ldots, N$, the ending diameters of the conical frustum ligaments are equal to $R_{yz}^{(k-1)}$ and $R_{yz}^{(k)}$ correspond to the $(k-1)$th and kth $y-z$ planes defined by Eq. (1):

$$R_{yz}^{(k-1)} = R_0 + \Delta R \left(\frac{k-1}{N} \right)^m \tag{2a}$$

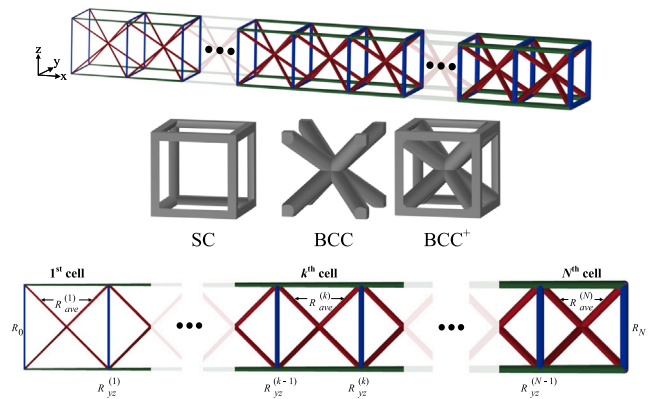$$R_{yz}^{(k)} = R_0 + \Delta R \left(\frac{k}{N} \right)^m \tag{2b}$$

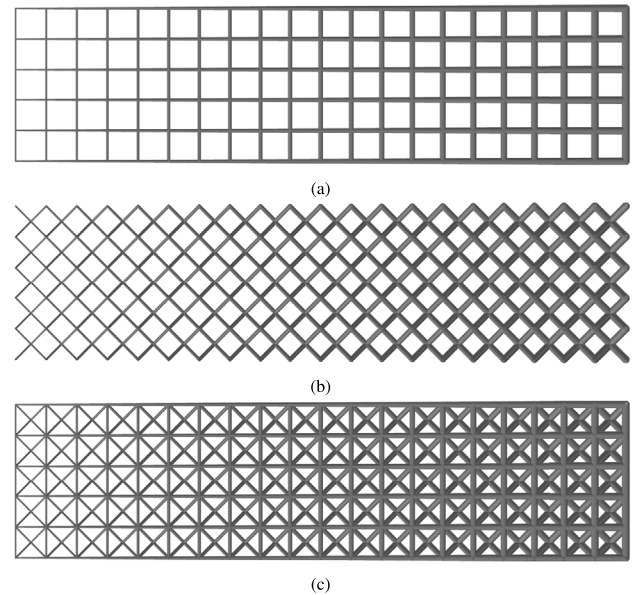**Fig. 1.** The schematic of the graded lattice structure and the three possible unit cells.

Fig. 2. Sample graded lattice structures with a linear ($m = 1$) variation of dimensionless diameter of ligaments R, from $R_0 = 0.05$ to $R_N = 0.25$ for (a) SC, (b) BCC and (c) BCC$^+$ unit cells.

The diameter of diagonal ligaments in kth cell is assumed to be constant and equals to the average diameter of the $(k-1)$th and kth $y-z$ planes as:

$$R_{ave}^{(k)} = \frac{R_{yz}^{(k-1)} + R_{yz}^{(k)}}{2} = R_0 + \frac{\Delta R}{2N^m}((k-1)^m + k^m) \tag{3}$$

It results in a step-wise change in the diameter of diagonal ligaments in N steps. Fig. 2 presents a sample of the three graded lattice structures with a linear power law variation, $m = 1$, from a thin to a thick dimensionless diameter, $R_0 = 0.05$ to $R_N = 0.5$, with a resolution of $N = 20$. As seen, for a linear variation swapping R_0 and R_N does not modify the geometry and the graded lattice only rotates 180°. However, this is not the case for $m \neq 1$. The effect of swapping $R_0 = 0.05$ and $R_N = 0.25$ on the geometry of a sample BCC$^+$ graded lattice is demonstrated in Fig. 3 for $m = 3$ resulting in a considerable difference in the variation of density and mechanical properties along the graded axis, x.

2.2. The relative density of graded lattices

The relative density of a cell is defined as the volume ratio of the lattice, ρ, to the bulk, ρ_0. It can be approximated based on the assumption that the volume of the lattice simply equals the sum of the
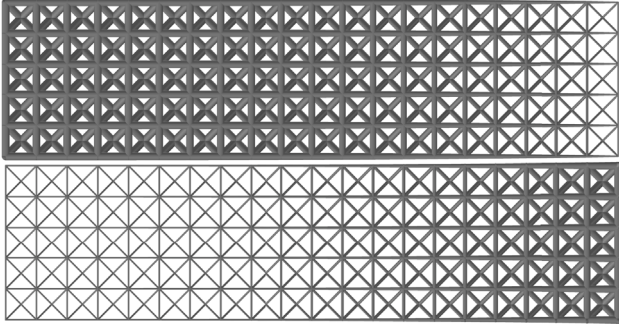
Fig. 3. The influence of swapping the values of $R_0 = 0.05$ and $R_N = 0.25$ for a graded BCC$^+$ lattice with $m = 3$.
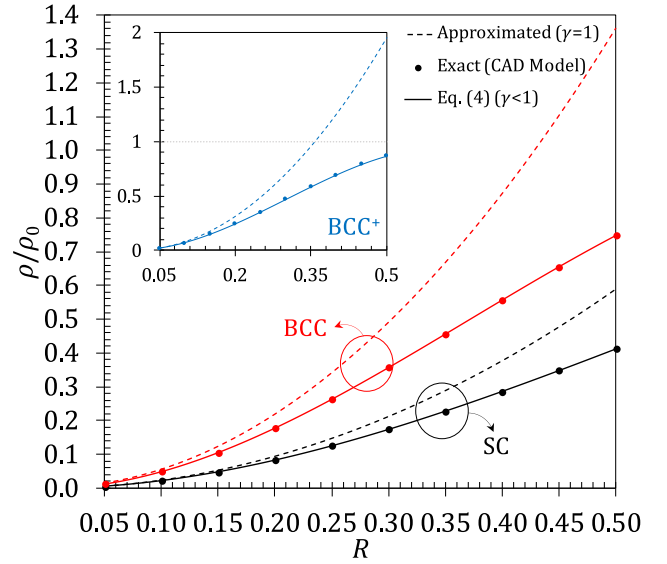

Fig. 4. Comparison of the modified relative density (Eq. (4) with $\gamma < 1$ obtained from the curve fitting to the CAD model) with the approximate one ($\gamma = 1$) for SC, BCC, and BCC$^+$ uniform lattices.

volume of the ligaments ignoring the overlaps in the joints (Gibson and Ashby, 2014), however, it overestimates the relative density, especially for higher values of R due to high overlapping volume. Hence, the correction factor, $\gamma < 1$ is introduced to fit the approximation to the exact values. For the special case of uniform unit cells with ligaments of identical diameter, it results in the following relative densities:

$$\left(\frac{\rho}{\rho_0}\right)^{(0)}_{SC} = \left(\frac{V_{cell}}{V_0}\right)^{(0)}_{SC} = \gamma_{SC}(3\pi/4)R^2 \tag{4a}$$

$$\left(\frac{\rho}{\rho_0}\right)^{(0)}_{BCC} = \left(\frac{V_{cell}}{V_0}\right)^{(0)}_{BCC} = \gamma_{BCC}\pi\sqrt{3}R^2 \tag{4b}$$

$$\left(\frac{\rho}{\rho_0}\right)^{(0)}_{BCC^+} = \left(\frac{V_{cell}}{V_0}\right)^{(0)}_{BCC^+} = \gamma_{BCC^+}\pi(3/4 + \sqrt{3})R^2 \tag{4c}$$

where V_{cell} is the total volume of ligaments without overlaps and $V_0 = l^3$ is the volume of the bulk unit cell (see Appendix A). For the SC lattice, a closed-form expression for evaluating the overlaps in an orthogonal junction of cylinders and consequently the exact value of γ_{SC} is available, however, for the BCC and BCC$^+$ lattices the least square approach is used to find the best fitted γ to the exact relative densities obtained from the exact CAD models:

$$\left(\frac{\rho}{\rho_0}\right)_{exact} = \gamma\left(\frac{\rho}{\rho_0}\right)_{approx} \tag{5a}$$

$$\gamma_{SC} = 1 - \frac{4\sqrt{2}}{3\pi}R \approx 1 - 0.600R \tag{5b}$$

$$\gamma_{BCC} = 1 - 0.900R \tag{5c}$$

$$\gamma_{BCC^+} = 1 - 1.1088R \tag{5d}$$

In Fig. 4 the approximation is compared to the exact relative density across the dimensionless diameter range of $0.05 < R < 0.5$ which reveals the undeniable error for $R > 0.2$

In a graded lattice, R is not constant and varies from R_0 to R_N via Eq. (1) with the power m. One can obtain the relative density of kth cell as a function of R_0 and ΔR as follows (for more details on the calculations see Appendix A):

$$\left(\frac{\rho}{\rho_0}\right)^{(k)}_{SC} = \gamma_{SC}^{(k)}\left[a_1^{(k)}R_0^2 + a_2^{(k)}(\Delta R)(R_0) + a_3^{(k)}\Delta R^2\right] \tag{6a}$$

$$\left(\frac{\rho}{\rho_0}\right)^{(k)}_{BCC} = \gamma_{BCC}^{(k)}\left[a_4^{(k)}R_0^2 + a_5^{(k)}(\Delta R)(R_0) + a_6^{(k)}\Delta R^2\right] \tag{6b}$$

$$\left(\frac{\rho}{\rho_0}\right)^{(k)}_{BCC^+} = \gamma_{BCC^+}^{(k)}\left[a_7^{(k)}R_0^2 + a_8^{(k)}(\Delta R)(R_0) + a_9^{(k)}\Delta R^2\right] \tag{6c}$$

where the coefficients $a_i^{(k)}$ are functions of k, the number of lattices along the graded direction, N, and the power m presented in Appendix A. To diminish the error caused by overlaps in the joints of graded lattices, the correction factor obtained for uniform unit cells in Eq. (5) is extended to the kth unit cell, $\gamma^{(k)}$, by substituting R with the average dimensionless diameter $R_{ave}^{(k)}$ defined in Eq. (3). Note that

Eq. (6) is simplified to the special case of uniform lattice presented in Eqs. (4) and (5) by setting either $\Delta R = 0$ or $m = 0$.

2.3. The analytical solution for relative elastic modulus of kth cell in the graded lattices

In this subsection, the analytical expression for the relative elastic modulus i.e., the stiffness ratio of the lattice, E, to the bulk, E_0, is presented based on the Euler–Bernoulli beam theory. For the graded lattices, the relative elastic modulus is not constant along the graded direction, x, due to the variation of dimensionless diameters of ligaments, R. Reminding Eqs. (1) and (3) which define the dimensionless diameter of the ligaments constructing the kth cell of the graded lattice, and a tapering variation in the diameter of the ligaments parallel to x, the relative elastic modulus for the kth unit cell is obtained by (see Appendix B for the details of calculations):

$$\left(\frac{E}{E_0}\right)^{(k)}_{SC} = \frac{\pi}{4}R_{yz}^{(k-1)}R_{yz}^{(k)} \tag{7a}$$

$$\left(\frac{E}{E_0}\right)^{(k)}_{BCC} = \pi\sqrt{3}\left(\frac{\left(R_{ave}^{(k)}\right)^4}{2 + \left(R_{ave}^{(k)}\right)^2}\right) \tag{7b}$$

$$\left(\frac{E}{E_0}\right)^{(k)}_{BCC^+} = \frac{b_1^{(k)}b_2^{(k)}}{b_1^{(k)} + b_2^{(k)}} \tag{7c}$$

where the coefficients $b_1^{(k)}$ and $b_2^{(k)}$ are presented in Appendix B. For the special case of uniform lattices with all the ligaments with identical dimensionless diameter, R, the relative stiffnesses of SC, BCC, and BCC$^+$ are:

$$\left(\frac{E}{E_0}\right)^{(0)}_{SC} = \frac{\pi}{4}R^2 \tag{8a}$$

$$\left(\frac{E}{E_0}\right)^{(0)}_{BCC} = \pi\sqrt{3}\left(\frac{R^4}{2 + R^2}\right) \tag{8b}$$

$$\left(\frac{E}{E_0}\right)^{(0)}_{BCC^+} = \frac{\pi}{4}\left(\left(1 + \frac{4\sqrt{3}}{9}\right)R^2 + \frac{8\sqrt{3}}{9}R^4\right) \tag{8c}$$
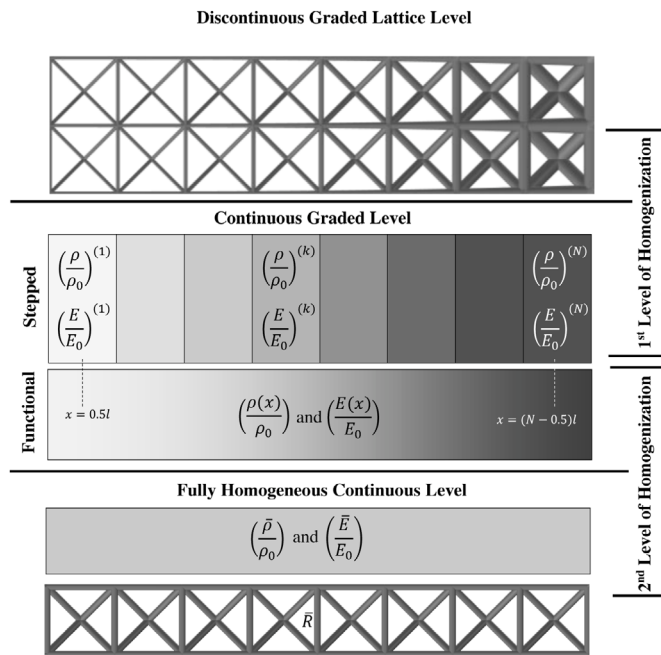
Discontinuous Graded Lattice Level

Fig. 5. The first and the second levels of homogenization of the graded lattices.

2.4. The equivalent function for density and elastic modulus of functionally graded lattices

A lattice structure is naturally a discontinuous non-homogeneous media and the exact value of density and elastic modulus at a given point (x, y, z) within the media is either the bulk density or zero according to whether the point is located on the ligaments or not (Fig. 5).

As the first level of homogenization, one can assume that the lattice structure within a unit cell space is a continuous homogeneous media with an equivalent density/modulus equal to the relative density/modulus of the cell, discussed respectively in Sections 2.2 and 2.3. However, as presented in Eqs. (6) and (7), the relative density, as well as the relative elastic modulus of the unit cells of a graded lattice structure, are not constant resulting in a step-wise variation along the direction of graduation which is x axis here (see Fig. 5). This subsection aims to suggest an approximation for the variation of relative density and relative elastic modulus as functions of x, i.e., $\rho(x)/\rho_0$ and $E(x)/E_0$. Since the variation of the diameters of ligaments with respect to x obeys a power law (Eq. (1)), the same form of approximation function is chosen:

$$\left(\frac{\rho(x)}{\rho_0}, \frac{E(x)}{E_0}\right) \approx (p_1, q_1) x^{(\alpha, \beta)m} + (p_2, q_2) \tag{9a}$$

$$(p_1, q_1) = \frac{\left(\frac{\rho}{\rho_0}, \frac{E}{E_0}\right)^{(N)} - \left(\frac{\rho}{\rho_0}, \frac{E}{E_0}\right)^{(1)}}{l^{(\alpha, \beta)m}((N-0.5)^{(\alpha, \beta)m} - 0.5^{(\alpha, \beta)m})} \tag{9b}$$

$$(p_2, q_2) = \left(\frac{\rho}{\rho_0}, \frac{E}{E_0}\right)^{(1)} - (0.5l)^{(\alpha, \beta)m} (p_1, q_1) \tag{9c}$$

where (,) represents *or* which means p_1, p_2, and α belongs to the density, while q_1, q_2, and β are related to the elastic modulus. In Eq. (9), the relative density/modulus of the first ($k = 1$) and the last ($k = N$) unit cells obtained from Eqs. (6) and (7) has assigned to the coordinate of their center, i.e., $x = 0.5l$, and $x = (N - 0.5)l$, see Fig. 5. The power m is modified by α and β fitting parameters as the variation of relative density/modulus with respect to x has not necessarily an identical power to the variation of the dimensionless diameter due to the discontinuous nature of the lattice. The calibrated values of α and β

corresponding to different values of R_0 and R_N for SC, BCC, and BCC$^+$ lattices are presented in both graphical forms and fitting equations in Appendix C.

2.5. The fully homogenized effective density and effective modulus of the graded lattices

The second possible level of homogenization for graded lattices is performed by introducing the effective density, $\bar{\rho}$, and the effective elastic modulus, $\bar{E}$, as shown in Fig. 5. $\bar{\rho}$ is the density of a fully homogenized material whose mass is equal to the mass of a graded lattice with N cells along the graded axis, while both of them have occupied the same volume of Nl^3. As the lattice structure is regular and all the cells have the same volume, l^3, the effective density, $\bar{\rho}$, is simply the average of the density of cells:

$$\frac{\bar{\rho}}{\rho_0} = \frac{1}{N} \sum_{k=1}^{N} \left(\frac{\rho}{\rho_0}\right)^{(k)} \tag{10}$$

which is divided by the bulk density, ρ_0, to be compatible with the representation in Eq. (6) for SC, BCC, and BCC$^+$ lattices. If the approximated continuous function for the density of graded lattice, $\rho(x)$ is used, Eq. (10) turns to an integration form:

$$\frac{\bar{\rho}}{\rho_0} \approx \frac{\int_0^{Nl} \left(\frac{\rho(x)}{\rho_0}\right) dx}{Nl} \tag{11}$$

Substituting Eq. (9) into Eq. (11) yields:

$$\frac{\bar{\rho}}{\rho_0} \approx \frac{p_1 (Nl)^{(\alpha m)}}{\alpha m + 1} + p_2 \tag{12}$$

After the first level of homogenization, the graded lattice converts to N unit cells with the elastic modulus of $E^{(k)}$, $k = 1, \ldots, N$, connected in series. Under an applied load in the grading direction, P, the total elongation of the graded structure is:

$$\delta_{graded} = \frac{Pl}{l^2} \sum_{k=1}^{N} \frac{1}{E^{(k)}} \tag{13}$$

The elongation of a fully homogenized material with the same cross-section area of l^2 and length Nl is:

$$\bar{\delta} = \frac{PNl}{l^2 \bar{E}} \tag{14}$$

One can find the effective modulus of the graded lattice by assuming $\delta_{graded} = \bar{\delta}$ and solving for $\bar{E}$:

$$\frac{\bar{E}}{E_0} = \frac{N}{\sum_{k=1}^{N} \frac{1}{(E/E_0)^{(k)}}} \tag{15}$$

which is divided by the bulk elastic modulus, E_0, to be compatible with the representation in Eq. (7) for SC, BCC, and BCC$^+$ lattices. The integration form of Eq. (15) can be obtained by using the continuous approximation of elastic modulus from Eq. (9) for evaluating the elongation of graded lattice, δ_{graded}, which results in:

$$\frac{\bar{E}}{E_0} \approx \frac{Nl}{\int_0^{Nl} \frac{1}{(E(x)/E_0)} dx} \tag{16}$$

Note that substituting Eq. (9) into Eq. (16) demands a numerical integration as the exact solution is not available.

It is useful to introduce a uniform lattice with a constant dimensionless diameter, $\bar{R}_\rho$, which results in the same effective relative density (same mass) by equating Eq. (12) to Eq. (4) considering the correction factor defined in Eq. (5) and solving for R:

$$\left(\frac{\bar{\rho}}{\rho_0}\right) = \left(\frac{\rho}{\rho_0}\right)^{(0)} \tag{17}$$

Similarly, the dimensionless diameter of a uniform lattice with the same effective relative modulus, $\bar{R}_E$, can be obtained by solving the following equation for R:

$$\left(\frac{\bar{E}}{E_0}\right) = \left(\frac{E}{E_0}\right)^{(0)} \tag{18}$$

The effective density and effective elastic modulus for SC, BCC, and BCC$^+$ lattices and for three different power, $m = 1$, 2, and 3 are graphically presented in Appendix D using the exact expressions in Eqs. (10) and (15).

2.6. The modified Gibson-Ashby model for graded lattices

According to the classical Gibson-Ashby model for a uniform cellular solid, the relative elastic modulus is related to the relative density as:

$$\left(\frac{E}{E_0}\right)^{(0)} = C^{(0)} \left(\left(\frac{\rho}{\rho_0}\right)^{(0)}\right)^{n^{(0)}} \tag{19}$$

where $C^{(0)}$ and $n^{(0)}$ are the fitting parameters. The modified Gibson-Ashby model is established based on the assumption that the original expression in Eq. (19) is also valid for the relationship between the effective relative modulus and the effective relative density given in Eqs. (10) and (15), respectively:

$$\left(\frac{\bar{E}}{E_0}\right) = \kappa C^{(0)} \left(\frac{\bar{\rho}}{\rho_0}\right)^{n^{(0)}} \tag{20}$$

in which κ is the correction factor that modifies the original relationship of uniform lattices for the graded ones. It is reasonable to assume that κ is a function f of the degree of gradual changes in the lattice geometry, which is controlled by the ratio (R_N/R_0) and the power m:

$$\kappa = f((R_N/R_0), m) \tag{21}$$

The calibrated values of κ are presented in Appendix E. The special case is when $(R_N/R_0) = 1$ or $m = 0$ resulting in a uniform lattice with $\kappa = 1$.

In addition to the fully homogenized effective properties, it is of interest to look at the graded lattice from a local (cell by cell) point of view, where the relative density and the relative elastic modulus vary along the graded direction, x, according to Eq. (9). One may suggest relating them to implementing the local version of the classical Gibson-Ashby model:

$$\left(\frac{E(x)}{E_0}\right) = C^{(0)} \left(\frac{\rho(x)}{\rho_0}\right)^{n^{(0)}} \tag{22}$$

However, another choice is to update the local version with the modified model by introducing the correction factor κ in Eq. (22):

$$\left(\frac{E(x)}{E_0}\right) = \kappa C^{(0)} \left(\frac{\rho(x)}{\rho_0}\right)^{n^{(0)}} \tag{23}$$

The comparison between the accuracy of Eqs. (22) and (23) for different combinations of the dimensionless diameters R_0, R_N, the power m, and for SC, BCC, and BCC$^+$ lattices is presented and discussed in Section 3.

2.7. The finite element method (FEM) validation study

Here, a numerical model based on FEM employing the commercial software, COMSOL Multiphysics®, is presented which is used to check the correctness and the validity of the developed analytical formulation. Two different sets of FEM simulations are performed: the unit cell simulations (FE-UC) and the lattice simulations (FE-Lattice). The FE-UC model considers the smallest representative structural element of the lattices, exactly the same as the assumption in Appendix B, by modeling the beam frames and the boundary conditions defined in Figs. B.2, B.3, and B.4 for the SC, BCC, and BCC$^+$ lattices, respectively. Due to its
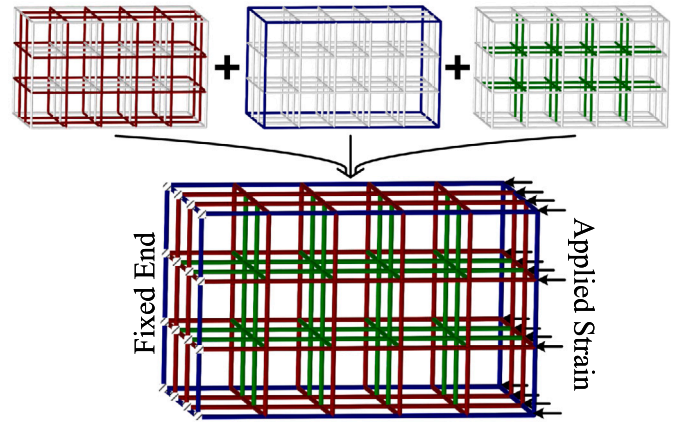

Fig. 6. The representative lattice of the FE-Lattice simulations.

unit cell-based approach, the FE-UC simulations are only applicable for checking the prediction of uniform lattices since the graded lattice needs a row of cells to define a graded change in the diameters of ligaments. To see the effect of shear deformation both Euler–Bernoulli and Timoshenko beam theories are applied to the FE-UC model. On the other hand, for the FE-Lattice simulations, a sample representative lattice consisting of 45 unit cells is modeled where $N = 5$ is the number of unit cells along the graded direction (and also load direction) and $3 \times 3 = 9$ unit cells are laid on the cross-sections. Fig. 6 presents the schematic of the representative lattice for the SC lattice.

It is assumed that the representative lattice is a section of a whole larger lattice and therefore, the ligaments on the outer skin are shared and do not completely belong to the representative lattice. Hence, the cross-section area of the ligaments on the lateral surfaces, the red ones, is divided by two (the diameter is divided by $\sqrt{2}$), while the cross-section area of the ligaments on the edges, the blue ones, is divided by four (the diameter is divided by 2). The cross-section of the ligaments within the representative lattice, green ones, is not modified. Note that for the BCC lattice, all the ligaments are within the lattice and are green. The boundary condition is applied as follows: For the 16 nodes on the right end of the lattice in Fig. 6, all the rotations are fixed and an arbitrary displacement along the graded direction, x, is applied. For the 16 nodes on the left end, all the rotations are fixed and the displacement along the x axis is fixed. Finally, for the rest of the boundary nodes on the lateral surfaces, the rotations are fixed. Since the developed analytical formulation is based on the Euler–Bernoulli beam theory, the same theory is employed for the FE-Lattice simulations. In both FE-UC and FE-Lattice simulations, every ligament with a circular cross-section is discretized by 10 quadratic meshes to guarantee independence from the mesh. Fig. 7 shows a sample of displacement field contours for the lattices with $R_N/R_0 = 3$ and $m = 1$.

The equivalent stress is calculated by dividing the resultant reaction force along the x axis on the fixed nodes on the left to the cross-section area of the model perpendicular to the x axis, and the equivalent strain is obtained by dividing the applied displacement by the length of the model along the x axis. Then, the effective modulus is calculated by dividing the equivalent stress by the equivalent strain.

3. Results and discussion

3.1. Analytical and numerical results

In this section, the validity of the proposed analytical model for graded lattices is examined and the question "How accurate is it to apply the classical Gibson-Ashby model with the coefficients obtained
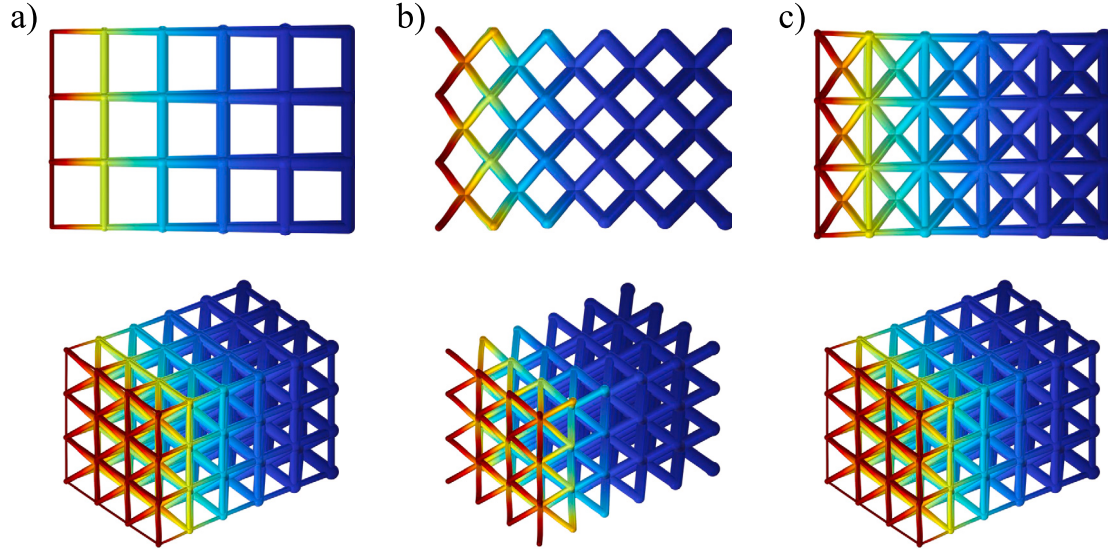
Fig. 7. Sample displacement fields along the applied strain direction from FEM-Lattice simulation for (a) SC, (b) BCC, and (c) BCC$^+$ lattices with $R_N/R_0 = 3$ and $m = 1$. The presented color maps are relative in order to show the distribution of the displacement field within the structure. Red represents the highest and blue is the lowest displacement.
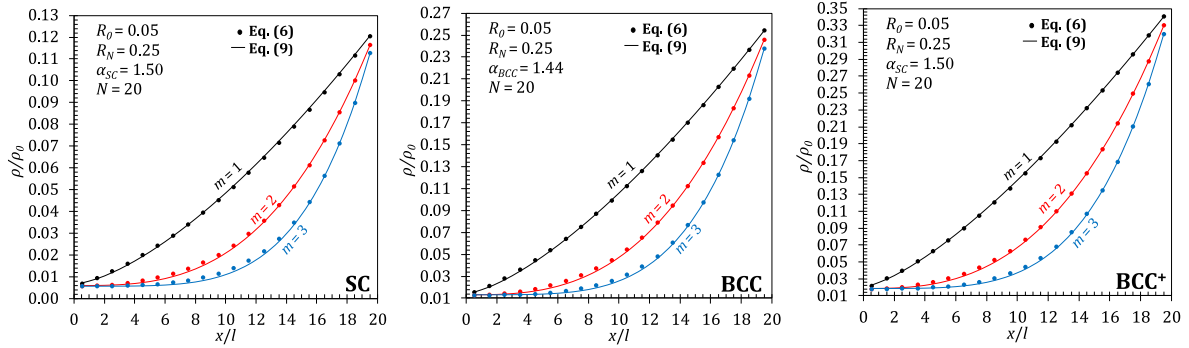

Fig. 8. The variation of relative density along the graded axis x and the accuracy test of the fitting function presented in Eq. (9).

from uniform lattices for graded lattices with the same unit cell type?" is answered.

First of all, the accuracy of the approximated continuous functions for variation of the relative density, $\rho(x)/\rho_0$, and relative elastic modulus, $E(x)/E_0$, along the graded direction, x, presented in Eq. (9), is studied. A high degree of variation of dimensionless diameter is considered by setting $R_0 = 0.05$, and $R_N = 0.25$ which means the diameter of ligaments increases 400% along the graded direction ($R_N/R_0 = 5$). Three different power for the variation function is assumed, $m = 1, 2$, and 3 to test the accuracy of Eq. (9) covering a broad range of changes in the geometry of the graded structure. Besides, the number of cells along the x axis is $N = 20$ to check the sensibility of approximated functions to the resolution of graded lattice, since the curve fitting parameters, α and β, presented in Appendix C are obtained from a high resolution of $N = 100$.

Fig. 8 compares the continuous function of relative density, $\rho(x)/\rho_0$, with the exact relative densities in Eq. (6) at the center of cells along x for SC, BCC, and BCC$^+$ lattices with the corresponding fitting parameters, $\alpha_{SC} = 1.5$, $\alpha_{BCC} = 1.44$, and $\alpha_{BCC^+} = 1.39$, which can be read from Fig. C.1 (Appendix C) with $R_0 = 0.05$, and $R_N = 0.25$. A good fitting is observed for all the lattices and the powers through the whole length of the graded lattice confirming the accuracy of Eq. (9) for evaluating the relative density even at a lower resolution, $N = 20$.

The same comparison is performed in Fig. 9 between the continuous function of relative elastic modulus, $E(x)/E_0$, with the exact relative

densities of cells presented in Eq. (7). The corresponding fitting parameters, $\beta_{SC} = 1.6$, $\beta_{BCC} = 2.94$, and $\beta_{BCC^+} = 1.65$ can be evaluated from Fig. C.2 (Appendix C). Again, a remarkable matching is seen which confirms the accuracy of Eq. (9) for the relative elastic modulus along the graded direction. Furthermore, the inverses of relative elastic modulus are compared in Fig. 9 for the three unit cells and one can perceive that $(E(x)/E_0)^{-1}$ does not match accurately the $((E/E_0)^{(k)})^{-1}$ especially for the BCC graded lattice. The reason is that the β values provided in Fig. C.2 (Appendix C) are obtained from the least square method in such a way that the total error between $((E/E_0)^{(k)})$ and $(E(x)/E_0)$ along the whole graded direction be minimized, which does not guaranty the best fitting for the inverses, particularly when the relative modulus is very low (the inverse is very high), as seen in the BCC lattice. Hence, one should notice that for the cases demanding the inverse of the function of relative modulus, such as $(E(x)/E_0)^{-1}$ in Eq. (16), another curve fitting with the values of inverse relative modulus as the input is needed to be performed to look for the updated values of the β parameter which are exclusively fitted on the inverse values.

Then, the coefficient $C^{(0)}$ and $n^{(0)}$ of the classical Gibson-Ashby model for the *uniform* SC, BCC, and BCC$^+$ lattices are obtained by fitting Eq. (19) to the relative elastic modulus and relative densities of uniform lattices presented in Eqs. (4) and (8), respectively. Fig. 10 depicts the output of the fitting and the corresponding calibrated coefficients. Note that the uniform dimensionless diameter, R, varies in the range of $0.05 < R < 0.5$ for both SC and BCC lattices resulting in a relative
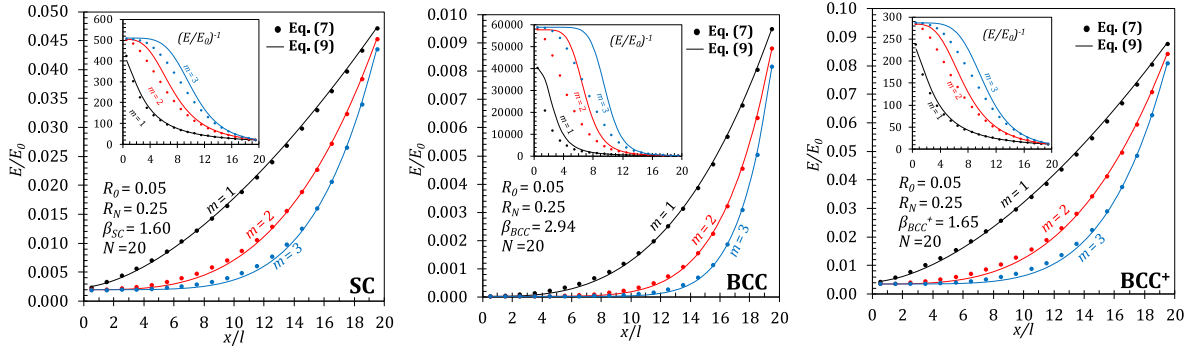
Fig. 9. The variation of elastic modulus along the graded axis x and the accuracy test of the fitting function presented in Eq. (9).
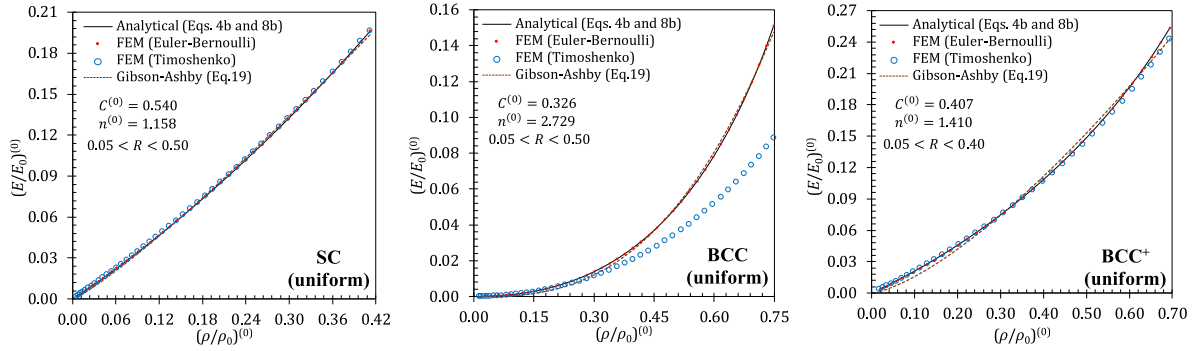

Fig. 10. The relative elastic modulus versus the relative density and the calibrated Gibson-Ashby model for the uniform lattices.
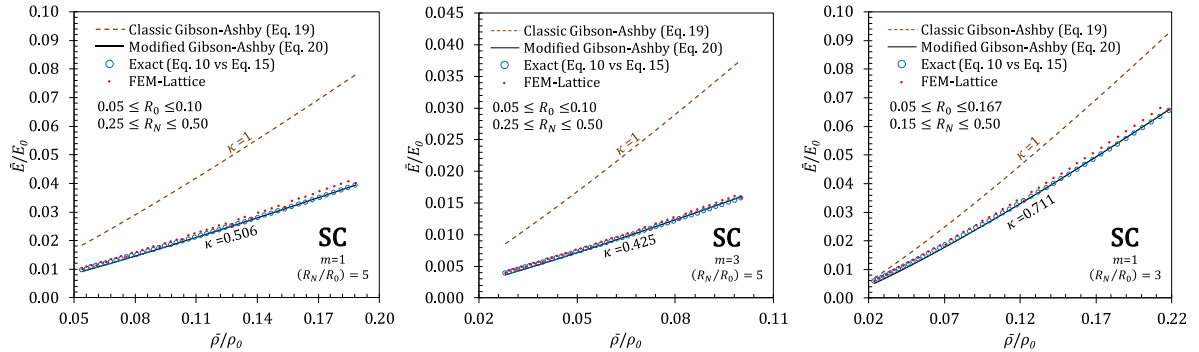

Fig. 11. The effective relative elastic modulus, $\bar{E}/E_0$, versus the effective relative density, $\bar{\rho}/\rho_0$ for the SC graded lattice.

density range of $0.0057 < (\rho/\rho_0)_{SC}^{(0)} < 0.412$ and $0.013 < (\rho/\rho_0)_{BCC}^{(0)} < 0.748$. However, the range for the BCC$^+$ lattice is limited to $0.05 < R < 0.4$ corresponding to the relative density range of $0.018 < (\rho/\rho_0)_{BCC^+}^{(0)} < 0.694$ to avoid a very high relative density of 0.869 for $R = 0.5$. A precise fitting of the power law Gibson-Ashby equation on the plot of analytical relative modulus versus relative density is observed, as expected. One should pay attention that the correction factor, $\gamma < 1$ introduced in Eq. (5), is applied to the calculated relative densities in Fig. 10, and it is the reason why the calibrated values differ from the approximated ones with $\gamma = 1$, for example, $C^{(0)} = 1/3$ and $n^{(0)} = 1$ for the uniform SC lattice by simply comparing Eqs. (4a) and (8a) (See Hedayati et al. (2016b)).

Besides, in Fig. 10 the relative elastic modulus obtained from FE-UC simulations based on both the Euler–Bernoulli and the Timoshenko beam theories are depicted. The Euler–Bernoulli remarkably fits the analytical prediction which confirms the correctness of the exact expression derived from the same theory, while the Timoshenko predicts lower elastic modulus for BCC and BCC$^+$ lattices where the shear

deformations play a role, particularly for BCC with all the ligaments inclined. The shear deformation effect grows by increasing R (thicker ligaments).

After that, the capability of the modified Gibson-Ashby model (Eq. (20)) in relating the effective relative modulus to the effective relative density and the accuracy of the correction factor, κ presented in Appendix E, is examined in Figs. 11, 12, and 13 for SC, BCC, and BCC$^+$ graded lattices, respectively. For each lattice, three cases of graded changes are inspected: The first two cases consider a high (400%, $(R_N/R_0) = 5$)) variation in the diameter of ligaments with $m = 1$ and $m = 3$ to also reveal the effect of power, while the last case assumes a lower (200% $(R_N/R_0) = 3$)) linear ($m = 1$) change in the diameters of ligaments along the graded direction. In all cases, the effective relative density is increased by increasing both R_0 and R_N proportionally to keep constant their ratio. The minimum of R_0 is 0.05 while the maximum of R_N is 0.5 for SC and BCC, and 0.4 for BCC$^+$ to avoid too high local relative densities (see the ranges of R_0 and R_N mentioned in the graphs). The exact values of effective elastic modulus
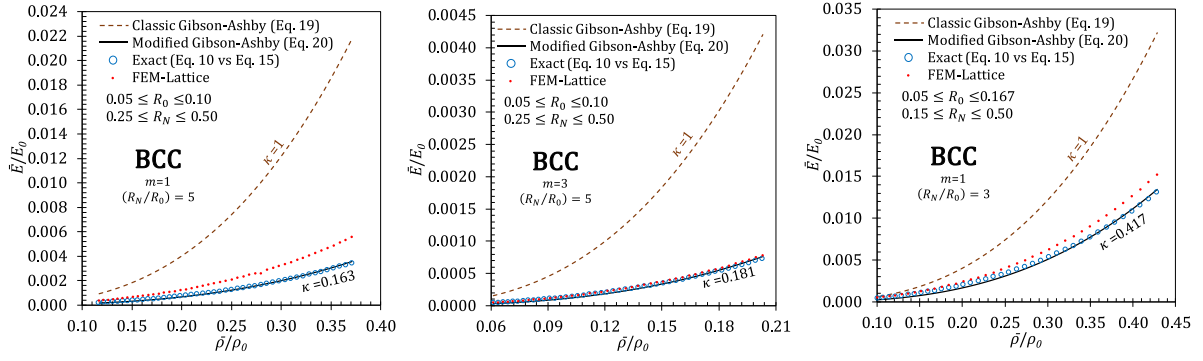
Fig. 12. The effective relative elastic modulus, $\bar{E}/E_0$, versus the effective relative density, $\bar{\rho}/\rho_0$ for the BCC graded lattice.
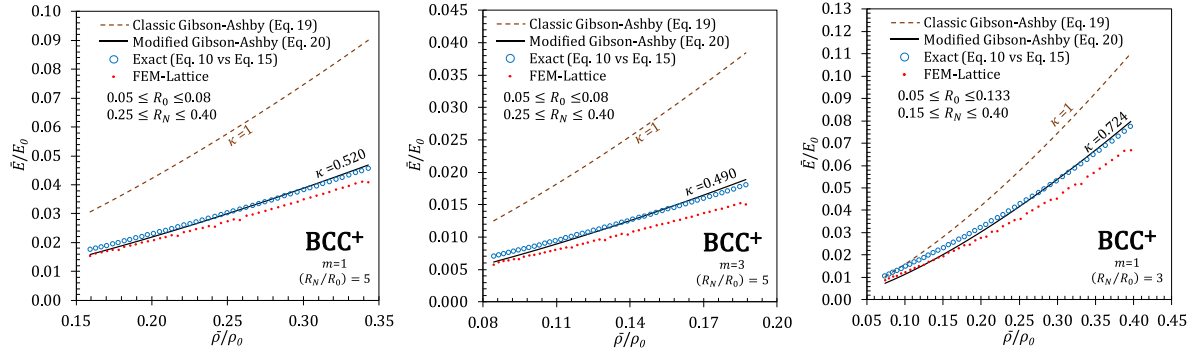

Fig. 13. The effective relative elastic modulus, $\bar{E}/E_0$, versus the effective relative density, $\bar{\rho}/\rho_0$ for the BCC$^+$ graded lattice.
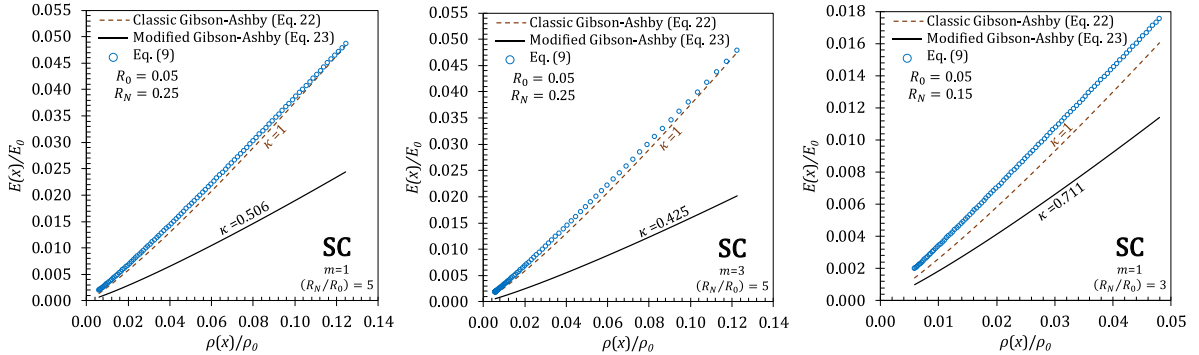

Fig. 14. The local (cell by cell) relative elastic modulus, $E(x)/E_0$, versus relative density, $\rho(x)/\rho_0$ for the SC graded lattice.

given by Eq. (10) are plotted versus the exact values of effective relative density Eq. (15) and the corresponding effective relative elastic modulus predicted by the classical (Fig. 10) and the modified (Eq. (20)) Gibson-Ashby models are plotted. First, it is proved that the classical model with the coefficients obtained from the fitting to the uniform lattices is not able to predict accurately the relationship between the effective properties of graded lattices. One can observe from Fig. E.1 that increasing the graded ratio, (R_N/R_0), causes the correction factor, κ, to be further away from the value of one, $\kappa = 1$, which means that the error between the original Gibson-Ashby model and the effective properties of the graded lattice structure is increasing. Accordingly, the error increases dramatically comparing the high graded ratio of $(R_N/R_0) = 3$ to the lower ratio $(R_N/R_0) = 3$. Second, it is confirmed that the calibrated correction factor, κ, is able to fit accurately the exact effective properties for all nine samples. Note that the calibrated correction factor of graded lattices is always lower than one, $\kappa < 1$, which rectifies the overestimation of the effective elastic modulus by the classical model with $\kappa = 1$ which is the worst for the BCC lattice. In

addition, the results obtained from FE-Lattice simulations introduced in Section 2.7 are plotted in Figs. 11, 12, and 13. These numerical simulations are close to the predictions of the modified Gibson-Ashby model which approves the need of introducing the modification into the classical model.

Finally, the question raised in Section 2.6, i.e., "Which of the classical or the modified Gibson-Ashby models fit better the local (cell by cell) relative modulus to the local relative density?" is answered. The variation of the local relative elastic modulus, $E(x)/E_0$, versus the local relative density, $\rho(x)/\rho_0$, both evaluated from Eq. (9), are compared to the local relative modulus predicted by the classical (Eq. (22)) and the modified (Eq. (23)) local Gibson-Ashby models in Figs. 14, 15, and 16 for SC, BCC, and BCC$^+$ graded lattices, respectively.

Three cases of study for each lattice are performed which indeed expand the first point of the plots in Figs. 11, 12, and 13) along the graded direction, x (see the values of R_0 and R_N mentioned in the graphs). It is seen that the classical formulation $\kappa = 1$ is more accurate from the local point of view compared to the modified version
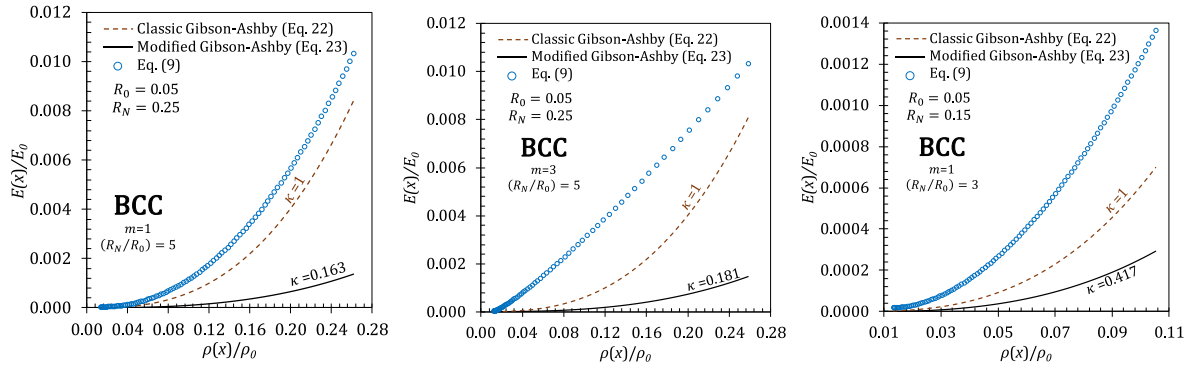
Fig. 15. The local (cell by cell) relative elastic modulus, $E(x)/E_0$, versus relative density, $\rho(x)/\rho_0$ for the BCC graded lattice.
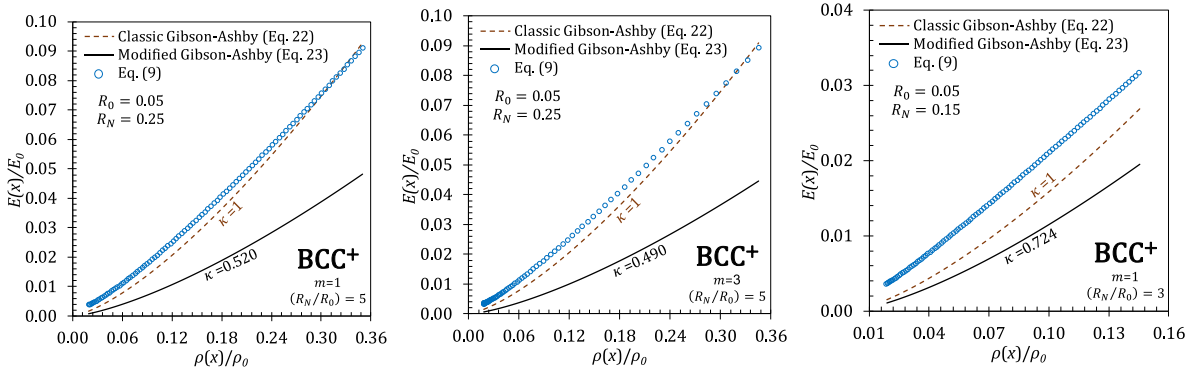

Fig. 16. The local (cell by cell) relative elastic modulus, $E(x)/E_0$, versus relative density, $\rho(x)/\rho_0$ for the BCC$^+$ graded lattice.
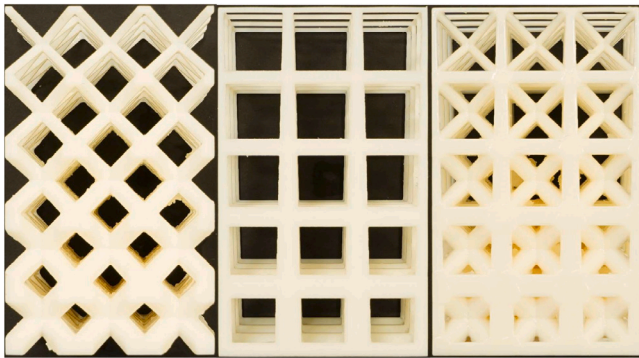

Fig. 17. The printed functionally graded lattice structure samples that were tested under compression loading. Right: BCC, center: SC and left: BCC$^+$.

calibrated using the overall effective properties. This is because, locally, each unit cell has almost a uniform structure, and therefore $\kappa = 1$ can better relate the properties cell by cell. Similar to the effective properties, the worst prediction of the classic and modified models belongs to the BCC lattice.

3.2. Experimental results

A set of experiments was performed to validate the analytical formulations derived in the previous section. The samples to be tested were printed by a Stratasys J750™ 3D printer using high-quality mode setting (resolution of 27 μm layer height and dimensional accuracy of 200 μm). A 3D printer exploiting a material-jetting technology was used since it allows obtaining almost isotropic samples with relatively small defects (Mora et al., 2022). A single configuration for each one

Fig. 18. The fabricated dog-bone samples uni-axially tested to estimate the mechanical properties of the bulk material (Vero PureWhite™) used to print the FG lattice structures.

of the considered unit cells was printed, namely a SC, BCC, and BCC$^+$. While the length of the unit cell is $l = 16$ mm, the $R_0 = 0.125$ and the $R_N = 0.375$ i.e. $d_0 = 2$ mm and $d_N = 6$ mm. The printed samples are shown in Fig. 17. It is worth mentioning that for the experimental models, $m = 1$ for all the models.

Table 1

Evaluated relative density $(\bar{\rho}/\rho_0)$ from the experimental tests and the corresponding analytical estimation.

	SC	BCC	BCC+
Exact (Eq. (4), $\gamma < 1$)	0.131	0.272	0.358
Experimental	0.145 ± 0.002	0.299 ± 0.014	0.394 ± 0.018
Approximate (Eq. (4), $\gamma = 1$)	0.160	0.367	0.527

Table 2

Evaluated relative effective modulus $(\bar{E}/E_0)$ from the experimental tests and the corresponding analytical results.

	SC	BCC	BCC+
Exact (Eq. (15))	0.0368	0.0075	0.0687
Experiments	0.0396 ± 0.0017	0.0062 ± 0.0003	0.0703 ± 0.0031
Modified Gibson-Ashby (Eq. (20))	0.0364	0.0069	0.0725
Classic Gibson-Ashby (Eq. (19))	0.0520	0.0093	0.0870

All samples were printed in Vero PureWhite™ material whose mechanical properties were estimated by specific uni-axial testing accordingly with ASTM-D638 (see Fig. 18). To perform these auxiliary tests, a constant strain rate of 0.1 mm/sec was imposed on the top cross-head of the loading frame machine (BETA 100 by MESSPHYSIK). From these tests, an average elastic modulus of $E_0 = 1436 \pm 10$ MPa has been estimated. A density $\rho_0 = 1.175$ g/cm^3 has been estimated for the bulk material.

To evaluate the effective elastic modulus of the 3D printed FG lattice structures, compression tests were conducted by imposing a constant strain rate of 0.1 mm/sec to the top face of the samples with a BETA 100 loading frame machine. Three tests were performed for each configuration, following ASTM-D638 standards. Prior to performing such compression tests, all the FG lattices were weighted to estimate their relative density $(\bar{\rho}/\rho_0)$ which is reported in Table 1. As can be seen from the results reported in this table, the correction factor γ in Eq. (4) allows to predict the relative density of the FG lattice structures with good accuracy as it excludes from the calculation of the overlapped volumes in the joints.

A comparison of the relative effective elastic modulus $(\bar{E}/E_0)$ obtained from the experiments with those obtained by the analytical model is shown in Table 2. It is noteworthy that the experimental tests exhibit minimal data scatter, with standard variations less than ± 5 in all cases. The reported relative elastic modulus values are the average of the three experimental data, demonstrating the reliability of the current approach for modifying the Gibson-Ashby model.

4. Conclusion

In this paper, a novel analytical framework for evaluating the mechanical properties of functionally graded lattices is developed where the relative density and consequently the relative elastic modulus vary along the graded direction due to gradual changes in the diameters of ligaments keeping constant the lattice parameter as a repetitive non-homogeneous structure. Three common cubic lattice system, i.e., simple cubic (SC), body-centered cubic (BCC), and their combination (BCC$^+$) are chosen as the geometry of unit cells. The first level of homogenization is accomplished by deriving an exact expression for the relative density and the relative elastic modulus of the kth cell along the graded direction performing a structural analysis of the representative beam frame of the unit cell including tapered beams. To ease of use in practical problems, continuous functions that approximate the variation of relative density and relative elastic modulus along the graded direction are introduced and fitted to the exact expressions at the center of cells via a least square approach in a broad range of changes in the geometry of the graded lattice. As the second level of homogenization, the exact expression for the effective relative density and the effective relative elastic modulus are derived to convert the graded lattice to a fully homogenized equivalent solid.

The modified Gibson-Ashby model is suggested to relate the effective relative modulus to the effective relative density of graded lattice by introducing a correction factor to the original equation since it is shown that the coefficients fitted to the uniform lattices cannot accurately fit the effective properties. The calibrated correction factor is presented for a wide range of possible geometries of the graded lattices in graphical form as well as approximated equations for the three lattices. Furthermore, it is proved that the classical model calibrated to uniform structures is able to match the local (cell by cell) relative elastic modulus to the local relative density along the graded direction. It suggests an ease-of-use practical framework for designing optimized graded lattice structures avoiding high-cost simulations and/or experimental measurements.

Funding

CRediT authorship contribution statement

Seyed Kamal Jalali: Conceptualization, Methodology, Formal analysis, Writing – original draft, Writing – review & editing. **Mohammad Javad Beigrezaee:** Software, Validation, Writing – original draft, Writing – review & editing, Visualization, Resources. **Diego Misseroni:** Writing – review & editing, Resources, Supervision, Funding acquisition. **Nicola Maria Pugno:** Conceptualization, Methodology, Formal analysis, Writing – review & editing, Supervision, Funding acquisition.

Declaration of competing interest

The authors declare that they have no known competing financial interests or personal relationships that could have appeared to influence the work reported in this paper.

Data availability

No data was used for the research described in the article.

Appendix A. Calculation of the relative density of kth cell

Consider the kth cell in a graded lattice that has three types of ligaments. The dimensionless diameter, R, of the first type of ligaments located on the $(k-1)$th and kth $y-z$ planes are defined in Eq. (2) and the dimensionless diameter of the second type ligaments which are parallel to x axis varies linearly from $R_{yz}^{(k-1)}$ to $R_{yz}^{(k)}$ forming four tapered ligaments. The dimensionless diameter of the third type, i.e., diagonal ligaments, is the average of $R_{yz}^{(k-1)}$ and $R_{yz}^{(k)}$ as explained in Eq. (3). To find the relative density, first, the ratio of the volume of a single ligament, V_{lig} to the volume of the cell, V_0 is needed for all three types. Note that the first and the third types have a cylindrical shape while the second type is a conical frustum. The volume ratio of a cylindrical ligament is:

$$\left(\frac{V_{lig}}{V_0}\right)_{cylinder} = \frac{(\pi/4)d^2\hat{l}}{l^3} \tag{A.1}$$

while for a tapered ligament with the ending diameters d_1 and d_2 it is:

$$\left(\frac{V_{lig}}{V_0}\right)_{taper} = \frac{(\pi/12)(d_1^2 + d_1 d_2 + d_2^2)\hat{l}}{l^3} \tag{A.2}$$

where $\hat{l} = l$ or $\hat{l} = \sqrt{3}l$ is the length of the ligament on the sides or on diagonals, respectively. Applying the dimensionless diameter

definition, $R = d/l$, the dimensionless form of the volume ratios of the ligaments constructing kth unit cell are obtained:

$$\left(\frac{V_{lig}}{V_0}\right)_{yz}^{(k-1)} = \frac{\pi}{4}\left(R_{yz}^{(k-1)}\right)^2 \tag{A.3a}$$

$$\left(\frac{V_{lig}}{V_0}\right)_{yz}^{(k)} = \frac{\pi}{4}\left(R_{yz}^{(k)}\right)^2 \tag{A.3b}$$

$$\left(\frac{V_{lig}}{V_0}\right)_{diagonal}^{(k)} = \frac{\pi\sqrt{3}}{4}\left(R_{ave}^{(k)}\right)^2 \tag{A.3c}$$

$$\left(\frac{V_{lig}}{V_0}\right)_{x}^{(k)} = \frac{\pi}{12}\left[\left(R_{yz}^{(k-1)}\right)^2 + R_{yz}^{(k-1)}R_{yz}^{(k)} + \left(R_{yz}^{(k)}\right)^2\right] \tag{A.3d}$$

Then, the relative density of the unit cell is given by summation over the volume ratio of all ligaments noticing that the ligaments on the sides are shared with the four adjacent cells while the diagonal ligaments exclusively belong to the cell. For SC, BCC, and BCC$^+$ lattices, it yields:

$$\left(\frac{\rho}{\rho_0}\right)_{SC}^{(k)} = \frac{4}{4}\left[\left(\frac{V_{lig}}{V_0}\right)_{yz}^{(k-1)} + \left(\frac{V_{lig}}{V_0}\right)_{yz}^{(k)} + \left(\frac{V_{lig}}{V_0}\right)_{x}^{(k)}\right] \tag{A.4a}$$

$$\left(\frac{\rho}{\rho_0}\right)_{BCC}^{(k)} = 4\left(\frac{V_{lig}}{V_0}\right)_{diagonal}^{(k)} \tag{A.4b}$$

$$\left(\frac{\rho}{\rho_0}\right)_{BCC^+}^{(k)} = \left(\frac{\rho}{\rho_0}\right)_{SC}^{(k)} + \left(\frac{\rho}{\rho_0}\right)_{BCC}^{(k)} \tag{A.4c}$$

Substituting Eqs. (2), (A.3), and (3) into Eq. (A.4) and some simplifications give the expression for relative density of kth cell of the graded SC, BC, and BCC$^+$ lattices:

$$\left(\frac{\rho}{\rho_0}\right)_{SC}^{(k)} = \left[a_1^{(k)}R_0^{\ 2} + a_2^{(k)}(\Delta R)(R_0) + a_3^{(k)}\Delta R^2\right] \tag{A.5a}$$

$$\left(\frac{\rho}{\rho_0}\right)_{BCC}^{(k)} = \left[a_4^{(k)}R_0^{\ 2} + a_5^{(k)}(\Delta R)(R_0) + a_6^{(k)}\Delta R^2\right] \tag{A.5b}$$

$$\left(\frac{\rho}{\rho_0}\right)_{BCC^+}^{(k)} = \left[a_7^{(k)}R_0^{\ 2} + a_8^{(k)}(\Delta R)(R_0) + a_9^{(k)}\Delta R^2\right] \tag{A.5c}$$

where the coefficients $a_i^{(k)}$ are:

$$a_1^{(k)} = 3\pi/4 \tag{A.6a}$$

$$a_2^{(k)} = a_1^{(k)}\frac{(k-1)^m + k^m}{N^m} \tag{A.6b}$$

$$a_3^{(k)} = a_1^{(k)}\frac{4(k-1)^{2m} + 4k^{2m} + k^m(k-1)^m}{9N^{2m}} \tag{A.6c}$$

$$a_4^{(k)} = \pi\sqrt{3} \tag{A.6d}$$

$$a_5^{(k)} = a_4^{(k)}\frac{(k-1)^m + k^m}{N^m} \tag{A.6e}$$

$$a_6^{(k)} = a_4^{(k)}\frac{((k-1)^m + k^m)^2}{4N^{2m}} \tag{A.6f}$$

$$a_7^{(k)} = a_1^{(k)} + a_4^{(k)} \tag{A.6g}$$

$$a_8^{(k)} = a_2^{(k)} + a_5^{(k)} \tag{A.6h}$$

$$a_9^{(k)} = a_3^{(k)} + a_6^{(k)} \tag{A.6i}$$

Appendix B. Calculation of the relative elastic modulus of kth cell

Here, the detailed calculations of relative elastic modulus for the kth cell of SC, BCC, and BCC$^+$ graded lattices based on Euler–Bernoulli beam theory are presented. The elongation of a bulk unit cell, δ_0 with the elastic modulus E_0 and the area $A_0 = l^2$ under an applied force, P, is:

$$\delta_0 = \frac{P}{lE_0} \tag{B.1}$$

Given the elongation of the lattice unit cell, δ under the same load, the relative elastic modulus of the cell is obtained, as shown in Fig. B.1:

$$\frac{E}{E_0} = \frac{\delta_0}{\delta} = \frac{P}{lE_0\delta} \tag{B.2}$$
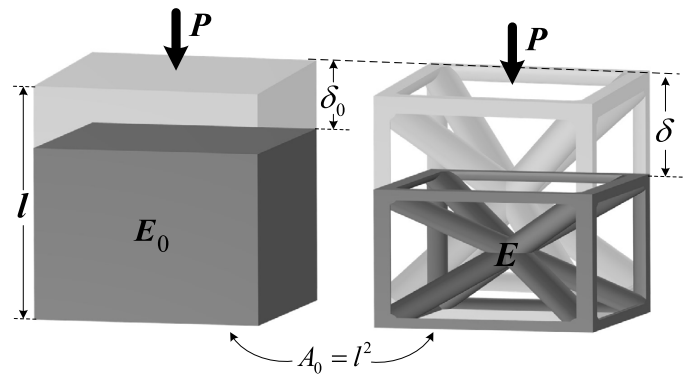

Fig. B.1. The schematic of comparison between the elongation of the bulk and the unit cell of graded lattice for finding the relative modulus by Eq. (B.2).
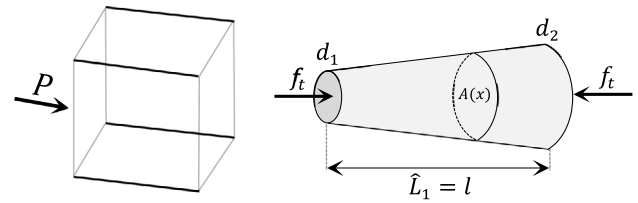

Fig. B.2. The tapered representative beam for calculating the relative density of the graded SC lattice.

SC graded lattice: In an SC unit cell, the ligaments on $y-z$ planes are not contributing when the load is applied along the x axis and the load is carried out by the four tapered ligaments parallel to x. For a tapered bar with the length $\hat{L}_1$ and the diameters of d_1 and d_2 under an applied axial load, f_t, the variable cross-section area, $A(x)$ and then the elongation, δ_{taper}, are:

$$A(x) = \frac{\pi}{4}\left(d_1 - (d_1 - d_2)(\frac{x}{\hat{L}_1})\right)^2 \tag{B.3a}$$

$$\delta_{taper} = \frac{f_t}{E_0}\int_0^{\hat{L}_1}\frac{1}{A(x)}\,dx = \frac{4f_t\hat{L}_1}{\pi E_0 d_1 d_2} \tag{B.3b}$$

Note that each of these ligaments is shared with four adjacent cells, and it means that every unit cell enjoys the benefit of one full tapered ligament in total, as shown in Fig. B.2. Hence, elongation of the SC unit cell with tapered lattice, δ_{SC}, is obtained by Setting $\hat{L}_1 = l$, and $f_t = P$ in Eq. (B.3b):

$$\delta_{SC} = \frac{4Pl}{\pi E_0 d_1 d_2} \tag{B.4}$$

Substituting Eq. (B.4) into Eq. (B.2) yields the relative density of the SC unit cell with tapered ligaments:

$$\left(\frac{E}{E_0}\right)_{SC,taper} = \frac{\pi}{4}\frac{d_1}{l}\frac{d_2}{l} \tag{B.5}$$

For the kth unit cell of the SC graded lattice, the diameter to length ratios in Eq. (B.5) are replaced with $R_{yz}^{(k-1)}$ and $R_{yz}^{(k)}$ resulting in:

$$\left(\frac{E}{E_0}\right)_{SC}^{(k)} = \frac{\pi}{4}R_{yz}^{(k-1)}R_{yz}^{(k)} \tag{B.6}$$

which is simplified to

$$\left(\frac{E}{E_0}\right)_{SC}^{(0)} = \frac{\pi}{4}R^2 \tag{B.7}$$

for a uniform SC lattice with identical ligaments' diameters.

BCC graded lattice: Taking the advantage of symmetry, only one-eighth of the unit cell, i.e., a single inclined ligament of length $\hat{L}_2 =$
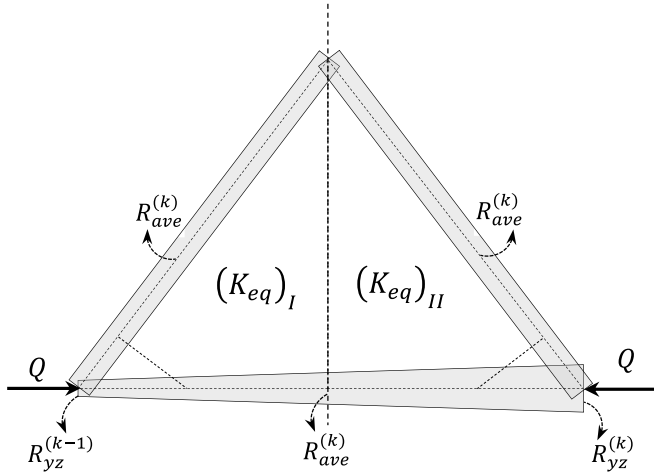
Fig. B.3. The Euler–Bernoulli beam model for calculating the relative density of the graded BCC lattice.

Fig. B.4. The Euler–Bernoulli beam model for calculating the relative density of the graded BCC$^+$ lattice.

$\sqrt{3}(l/2)$ carrying a quarter of unit cell load, $P/4$, is considered in the analytical solution to find the elongation of the BCC unit cell (see Fig. B.3). Since the joints are assumed to be rigid, the slopes of the ligament at both ends are zero. The applied load, P is decomposed to its components, f_η and f_ζ, along the local axial, η, and transverse, ζ coordinate of the ligament:

$$f_\eta = \frac{\sqrt{3}}{3} P \tag{B.8a}$$

$$f_\zeta = \frac{\sqrt{2}}{\sqrt{3}} P \tag{B.8b}$$

To keep the slope zero, an additional moment, $M_z = f_\zeta \hat{L}_2/2$, is applied from the rigid joint. It results in an axial, u_η, and a transverse, u_ζ, displacement at the free tip of the ligament:

$$u_\eta = \frac{f_\eta \hat{L}_2}{A E_0} \tag{B.9a}$$

$$u_\zeta = \frac{f_\zeta \hat{L}_2^3}{12 E_0 I} \tag{B.9b}$$

where $A = (\pi/4)d^2$ and $I = (\pi/64)d^4$ for the circular cross-section. Then, the displacement of the ligament tip along the load P, i.e., x axis, is calculated as:

$$u_x = \frac{\sqrt{3}}{3} u_\eta + \frac{\sqrt{2}}{\sqrt{3}} u_\zeta \tag{B.10}$$

Substituting Eqs. (B.9), (B.8), into Eq. (B.10) gives the total elongation of the BCC unit cell, δ_{BCC} as the twice of u_x:

$$\delta_{BCC} = 2u_x = \frac{P}{\sqrt{3}\pi E_0} \left(\frac{l}{d^2} + 2\frac{l^3}{d^4} \right) \tag{B.11}$$

Substituting Eq. (B.11) into Eq. (B.2) yields the relative elastic modulus:

$$\left(\frac{E}{E_0} \right)_{BCC}^{(0)} = \pi \sqrt{3} \left(\frac{R^4}{2 + R^2} \right) \tag{B.12}$$

The relative elastic modulus of kth unit cell of the BCC lattice is simply given by replacing R with $R_{ave}^{(k)}$ since it is assumed that the diagonal ligaments are cylindrical:

$$\left(\frac{E}{E_0} \right)_{BCC}^{(k)} = \pi \sqrt{3} \left(\frac{\left(R_{ave}^{(k)} \right)^4}{2 + \left(R_{ave}^{(k)} \right)^2} \right) \tag{B.13}$$

BCC$^+$ graded lattice: The representative frame of the BCC$^+$ lattice for the analytical calculation consists of four inclined ligaments of length $\hat{L}_2 = (\sqrt{3}/2)l$, the diameter d_3, a tapered ligament with length $\hat{L}_1 = (l/2)$ and ending diameters d_1 and d_2. The connecting joint moves only along the x axis because of the symmetry of the inclined ligaments and the fact that the tapered one must remain straight. The schematic of this representative frame is displayed in Fig. B.4, while for better visibility only one of four inclined ligaments is depicted.

Here, a unity displacement, $u_x = 1$ is applied to the connecting joint and the equivalent required the corresponding load, Q is evaluated from the equilibrium which is equal to the effective stiffness of the frame, K_{eq}:

$$Q = K_{eq} u_x = K_{eq} \tag{B.14}$$

The applied unity displacement causes a unity elongation of tapered ligament and a reaction force, f_t, along the x axis. This reaction force

Fig. B.5. The Euler–Bernoulli beam model for calculating the relative density of the graded BCC$^+$ lattice.

is obtained from Eq. (B.3b) by setting $\delta_{taper} = 1$ and solving for f_t:

$$f_t = \frac{\pi E_0 d_1 d_2}{4 \hat{L}_1} \tag{B.15}$$

Besides, it imposes an axial displacement, $u_\eta = (\sqrt{3}/3)$, and a transverse displacement, $u_\zeta = (\sqrt{2}/\sqrt{3})$ to each inclined ligament. Replacing these values to Eq. (B.9) and solving for f_η and f_ζ, gives the reaction forces of each inclined ligament on the joint:

$$f_\eta = \frac{\sqrt{3}}{3} \frac{A E_0}{\hat{L}_2} \tag{B.16a}$$

$$f_\zeta = \frac{\sqrt{2}}{\sqrt{3}} \frac{12 E_0 I}{\hat{L}_2^3} \tag{B.16b}$$

The equilibrium along the x axis gives the force Q which results in the assumed unity displacement:

$$Q = f_t + 4 \frac{\sqrt{3}}{3} f_\eta + 4 \frac{\sqrt{2}}{\sqrt{3}} f_\zeta \tag{B.17}$$

Substituting Eqs. (B.15), (B.16), and (B.14) into Eq. (B.17) and setting $\hat{L}_1 = l/2$, $\hat{L}_2 = (\sqrt{3}/2)l$, $A = (\pi/4)d_3^2$, and $I = (\pi/64)d_3^4$, yields the equivalent stiffness of the frame:

$$K_{eq} = \frac{\pi l E_0}{2} \left(\frac{d_1}{l} \frac{d_2}{l} + \frac{4\sqrt{3}}{9} \left(\left(\frac{d_3}{l} \right)^2 + 2 \left(\frac{d_3}{l} \right)^4 \right) \right) \tag{B.18}$$

The kth unit cell of the BCC$^+$ lattice can be assumed as a combination of two frames, I and II, assembled in series. In the frame I, the dimensionless diameters are $R_1 = (d_1/l) = R_{yz}^{(k-1)}$, $R_2 = (d_2/l) = R_{ave}^{(k)}$, and $R_3 = (d_3/l) = R_{ave}^{(k)}$, while for the frame II, they are $R_1 = (d_1/l) = R_{ave}^{(k)}$, $R_2 = (d_2/l) = R_{ave}^{(k)}$, and $R_3 = R_{yz}^{(k1)}$ (see Fig. B.5). Replacing these dimensionless diameters in Eq. (B.18), the effective stiffness of these two frames is calculated as:

$$(K_{eq})_I = \frac{\pi l E_0}{2} \left(R_{yz}^{(k-1)} R_{ave}^{(k)} + \frac{4\sqrt{3}}{9} \left(\left(R_{ave}^{(k)} \right)^2 + 2 \left(R_{ave}^{(k)} \right)^4 \right) \right) \tag{B.19a}$$

$$(K_{eq})_{II} = \frac{\pi l E_0}{2} \left(R_{ave}^{(k)} R_{yz}^{(k)} + \frac{4\sqrt{3}}{9} \left(\left(R_{ave}^{(k)} \right)^2 + 2 \left(R_{ave}^{(k)} \right)^4 \right) \right) \tag{B.19b}$$

and the total effective stiffness of the unit cell, $(K_{eq})_{BCC^+}$, is the combination of these two springs in series:

$$(K_{eq})_{BCC^+} = \frac{(K_{eq})_I (K_{eq})_{II}}{(K_{eq})_I + (K_{eq})_{II}} \tag{B.20}$$

Having the total stiffness of the unit cell, its elongation due to the applied load P is obtained as:

$$\delta_{BCC^+} = \frac{P}{(K_{eq})_{BCC^+}} \tag{B.21}$$

Then, replacing this elongation in Eq. (B.2) yields the relative stiffness of the BCC$^+$ unit cell:

$$\left(\frac{E}{E_0} \right)_{BCC^+} = \frac{b_1^{(k)} b_2^{(k)}}{b_1^{(k)} + b_2^{(k)}} \tag{B.22}$$

where

$$b_1^{(k)} = \frac{\pi}{2} \left(R_{yz}^{(k-1)} R_{ave}^{(k)} + \frac{4\sqrt{3}}{9} \left(\left(R_{ave}^{(k)} \right)^2 + 2 \left(R_{ave}^{(k)} \right)^4 \right) \right) \tag{B.23a}$$

$$b_2^{(k)} = \frac{\pi}{2} \left(R_{ave}^{(k)} R_{yz}^{(k)} + \frac{4\sqrt{3}}{9} \left(\left(R_{ave}^{(k)} \right)^2 + 2 \left(R_{ave}^{(k)} \right)^4 \right) \right) \tag{B.23b}$$

For the special case of uniform BCC$^+$ unit cell with the ligaments of identical dimensionless diameter, R, the coefficients $b_1^{(k)}$ and $b_2^{(k)}$ are equal and independent from k and the relative elastic modulus simplifies to:

$$\left(\frac{E}{E_0} \right)_{BCC^+}^{(0)} = \frac{\pi}{4} \left(\left(1 + \frac{4\sqrt{3}}{9} \right) R^2 + \frac{8\sqrt{3}}{9} R^4 \right) \tag{B.24}$$

Appendix C. Curve fitting parameters α and β for the equivalent density and modulus

Figs. C.1 and C.2, illustrate the curve fitting parameters α and β defined in Eq. (9) for the continuous functions of relative density and relative modulus for SC, BCC, and BCC$^+$ graded lattices. Graphs are presented for a wide range of dimensionless diameter combinations, i.e., $R_0 = 0.05, 0.07, 0.1, 0.12, 0.14, 0.17, 0.21, 0.25$, and 0.3, and for each $R_0 < R_N < 0.5$. The presented α and β parameters are obtained by the best fitting of Eq. (9) to Eq. (6) and Eq. (7) for a high-resolution graded lattice with $N = 100$ implementing the least square approach. For intermediate values of R_0 which are not presented in Figs. C.1 and C.2 one can obtain the α and β parameters via interpolation or use the

Table C.3
The dimensionless constants for Eq. (C.1).

	α_{SC}	α_{BCC}	α_{BCC^+}	β_{SC}	β_{BCC}	β_{BCC^+}
A_1	−12.100	−11.880	−11.850	−12.480	−40.910	−12.480
A_2	59.660	59.110	58.220	61.040	197.800	60.670
A_3	−114.200	−111.700	−103.400	−117.300	−174.400	−118.200
A_4	93.460	89.070	62.650	91.530	−114.100	92.800
A_5	−27.070	−24.390	6.417	−23.810	72.050	−23.580
B_1	9.306	9.081	8.769	9.688	31.900	9.687
B_2	−46.610	−46.850	−46.400	−45.510	−154.900	−44.540
B_3	116.500	115.900	114.400	112.800	356.300	113.000
B_4	−150.800	−149.800	−148.600	−144.300	−400.200	−145.300
B_5	78.840	77.760	76.540	75.020	176.700	75.580
C_1	−97.510	−90.840	−96.230	−103.600	13.600	−106.700
C_2	−130.300	−137.900	−145.300	−142.100	−983.100	−139.900
C_3	−49.620	−47.240	−70.660	−32.120	−417.100	−30.700
C_4	87.770	84.870	69.200	89.350	706.500	87.930
C_5	229.100	229.400	239.800	245.900	946.500	247.300
C_6	147.100	148.000	168.000	134.000	1177.000	130.100
C_7	−122.100	−120.300	−96.850	−131.300	−980.900	−129.000
C_8	−151.600	−151.900	−159.000	−153.000	−884.000	−151.200
C_9	44.490	43.130	29.820	53.120	362.200	52.020
C_{10}	12.550	13.280	16.660	9.983	40.650	9.386
D	1.090	1.104	1.116	1.090	1.324	1.095

following simplified approximation (see Table C.3):

$$
\begin{aligned}
\alpha, \beta =\ & A_1 R_0 + A_2 R_0^2 + A_3 R_0^3 + A_4 R_0^4 + A_5 R_0^5 \\
& + B_1 R_N + B_2 R_N^2 + B_3 R_N^3 + B_4 R_N^4 + B_5 R_N^5 \\
& + C_1 R_0^4 R_N + C_2 R_0^3 R_N^2 + C_3 R_0^2 R_N^3 + C_4 R_0 R_N^4 \\
& + C_5 R_0^3 R_N + C_6 R_0^2 R_N^2 + C_7 R_0 R_N^3 \\
& + C_8 R_0^2 R_N + C_9 R_0 R_N^2 \\
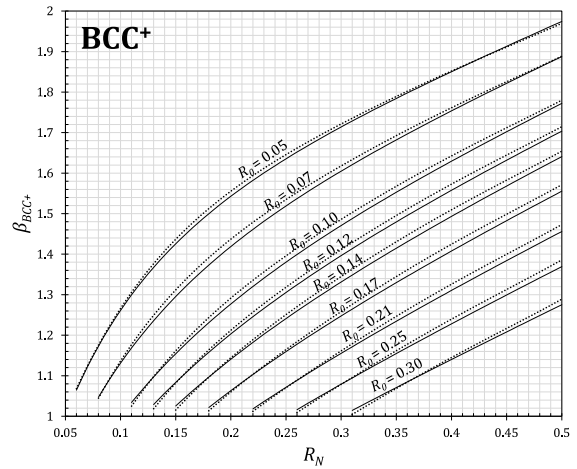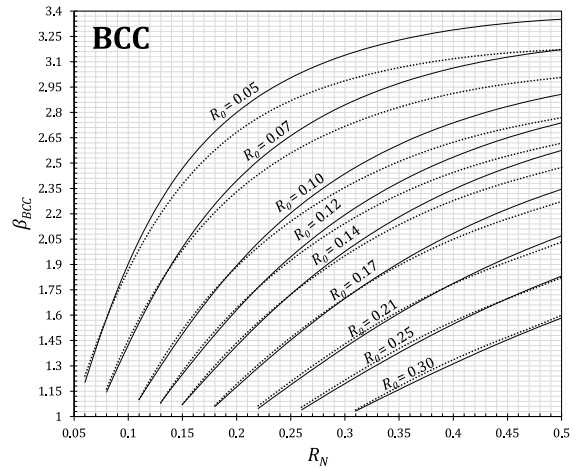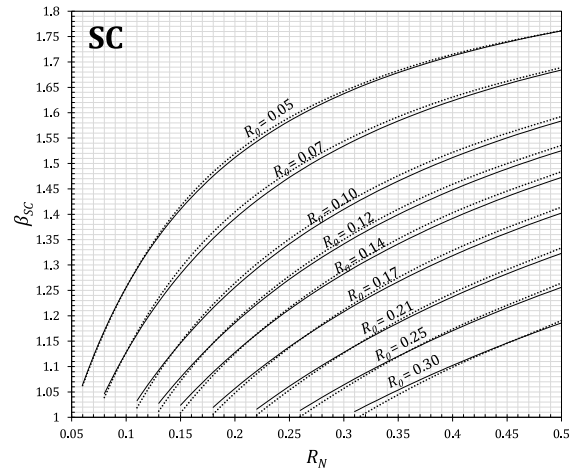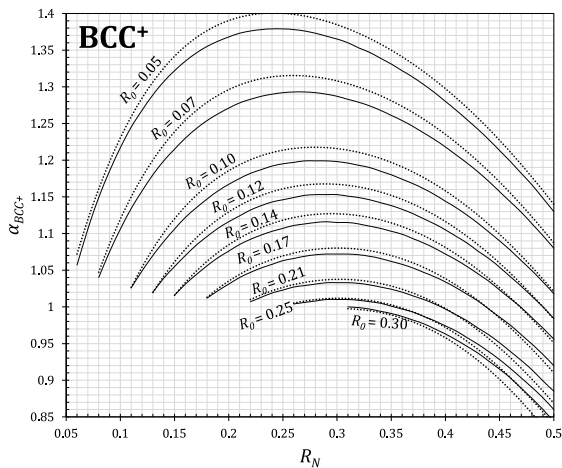& + C_{10} R_0 R_N + D
\end{aligned}
\tag{C.1}
$$
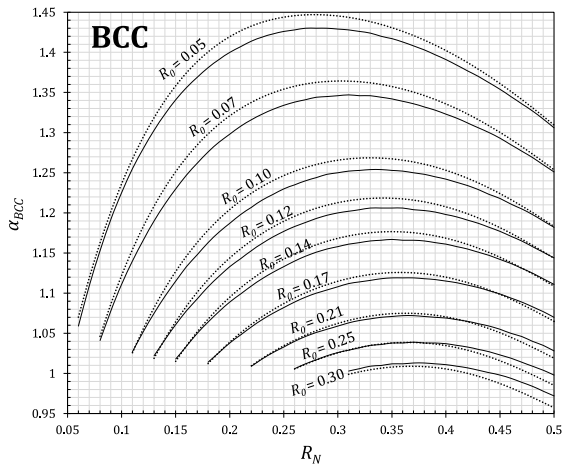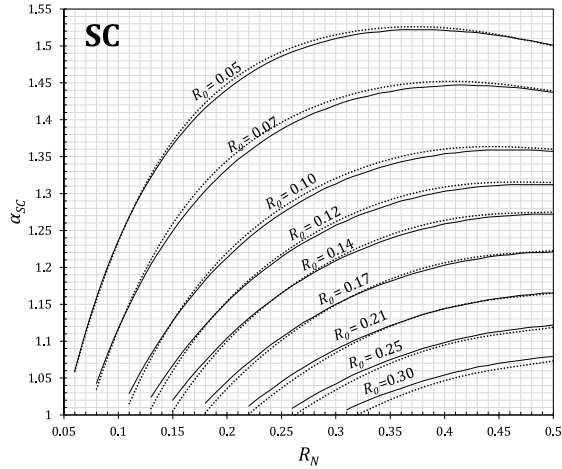
Fig. C.1. The curve fitting parameter α for SC, BCC, and BCC⁺. Dashed lines are from Eq. (C.1).

Fig. C.2. The curve fitting parameter β for SC, BCC, and BCC⁺. Dashed lines are from Eq. (C.1).

Appendix D. Graphical presentation of effective modulus and effective density of graded lattices

Figs. D.1 to D.6, depict the relative effective density and the relative effective elastic modulus of fully homogenized SC, BCC, and BCC$^+$ graded lattices according to the exact series expressions in Eq. (10)

and Eq. (15). Graphs are presented for three different powers for grading, $m = 1$, 2, and 3, and a wide range of dimensionless diameter combinations, i.e., $R_0 = 0.05$, 0.1, 0.15, 0.2, 0.25, and 0.3, and for each $R_0 < R_N < 0.5$, which can be used as a design guide for tuning the effective properties of the graded lattice.
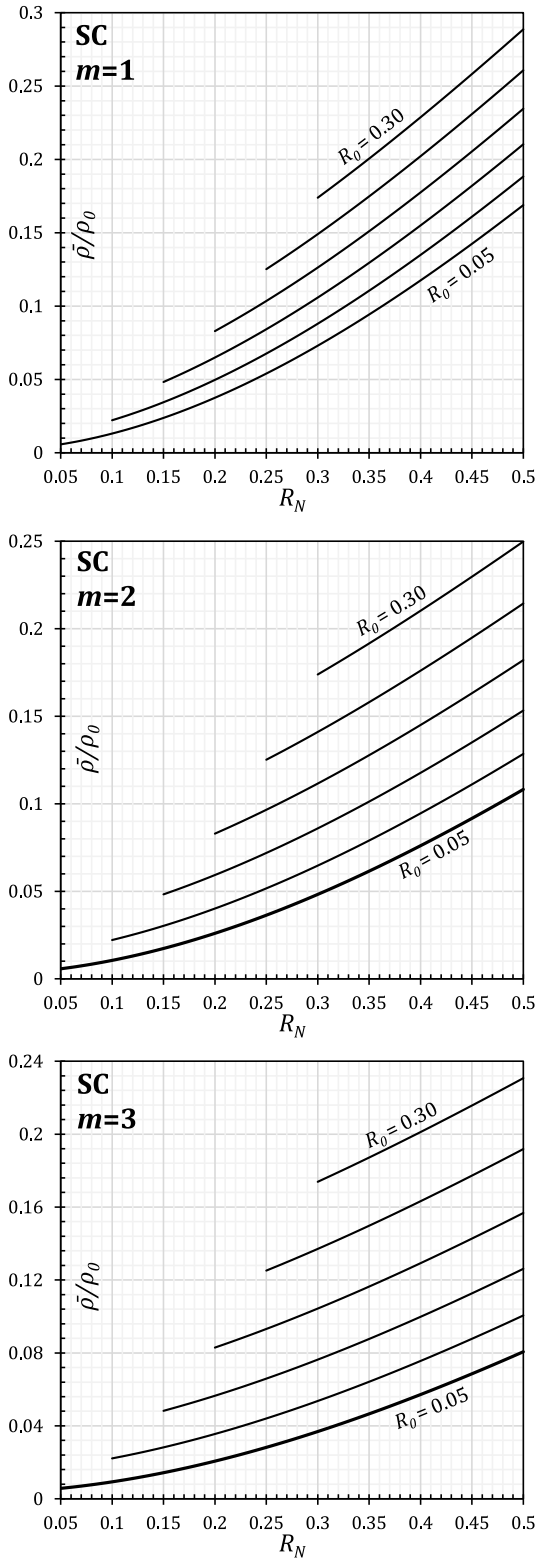
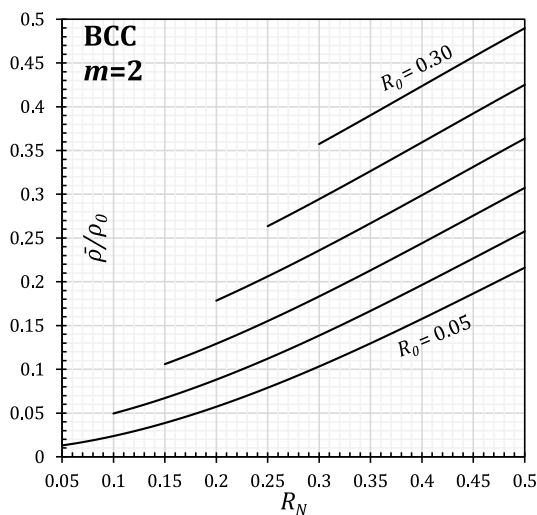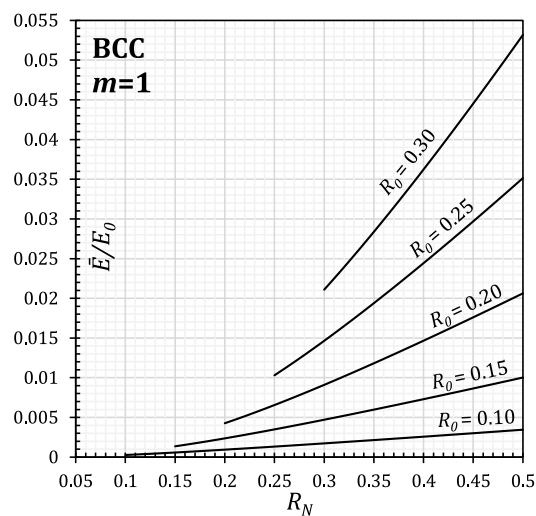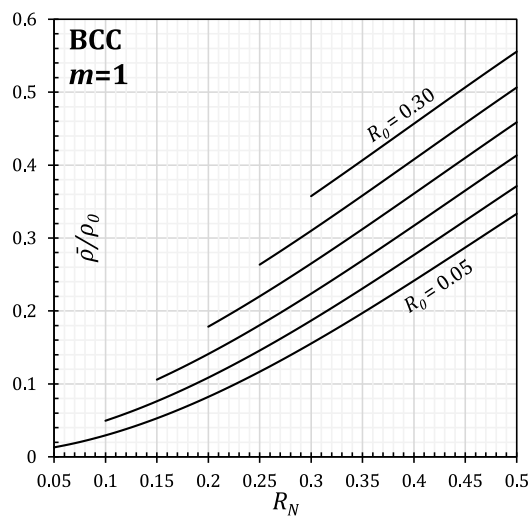**Fig. D.1.** The relative effective density of SC lattices for the power $m = 1$, 2, and 3, and different values of R_0 and R_N.
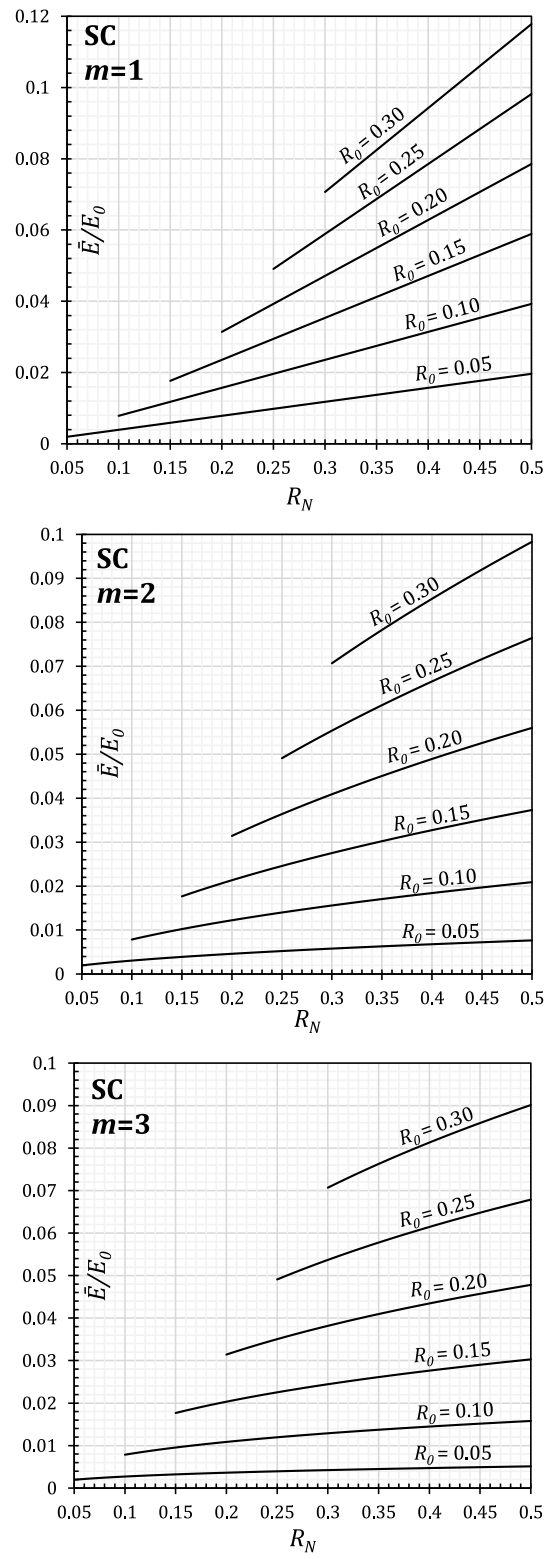
Fig. D.2. The relative effective elastic modulus of SC lattices for the power $m = 1$, 2, and 3, and different values of R_0 and R_N.
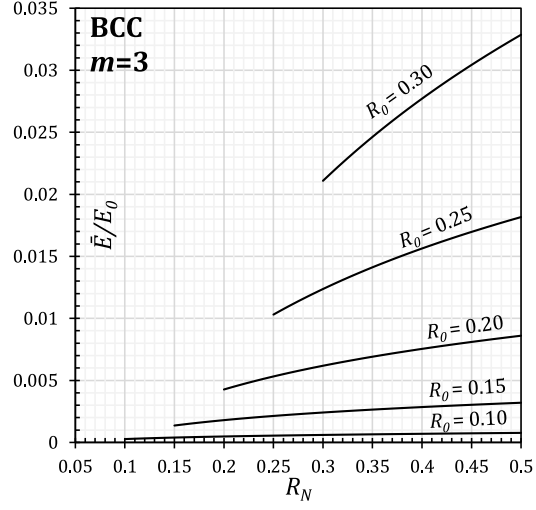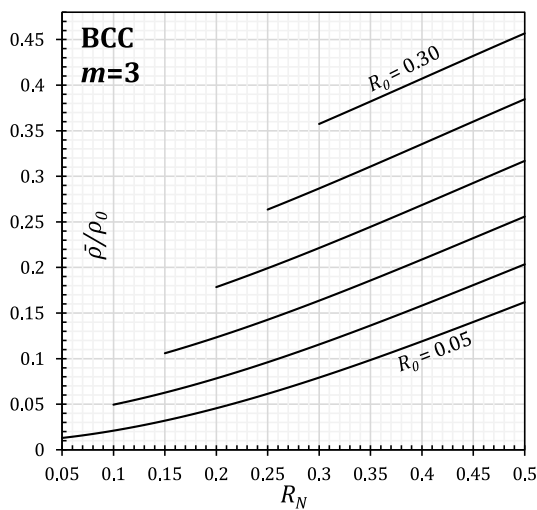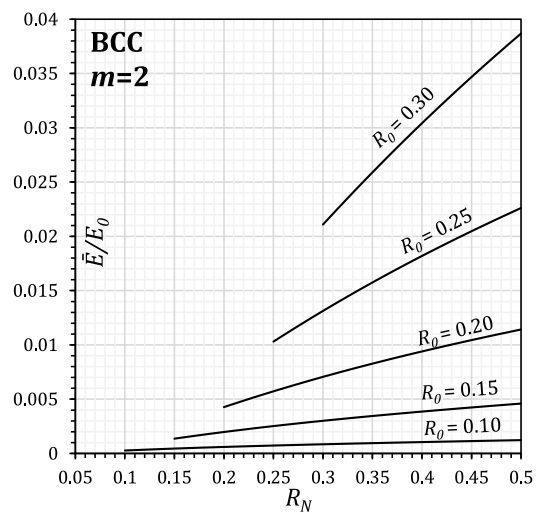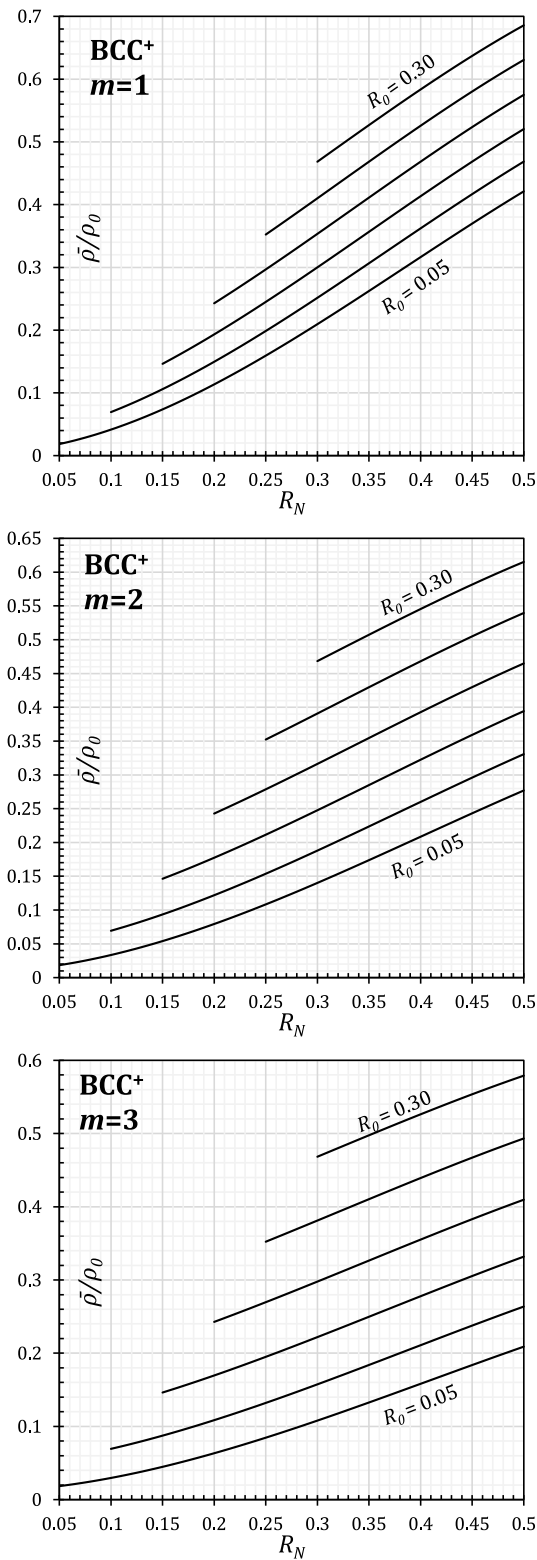
Fig. D.3. The relative effective density of BCC lattices for the power $m = 1$, 2, and 3, and different values of R_0 and R_N.

Fig. D.4. The relative effective elastic modulus of BCC lattices for the power $m = 1$, 2, and 3, and different values of R_0 and R_N.

Fig. D.5. The relative effective density of BCC⁺ lattices for the power $m = 1$, 2, and 3, and different values of R_0 and R_N.
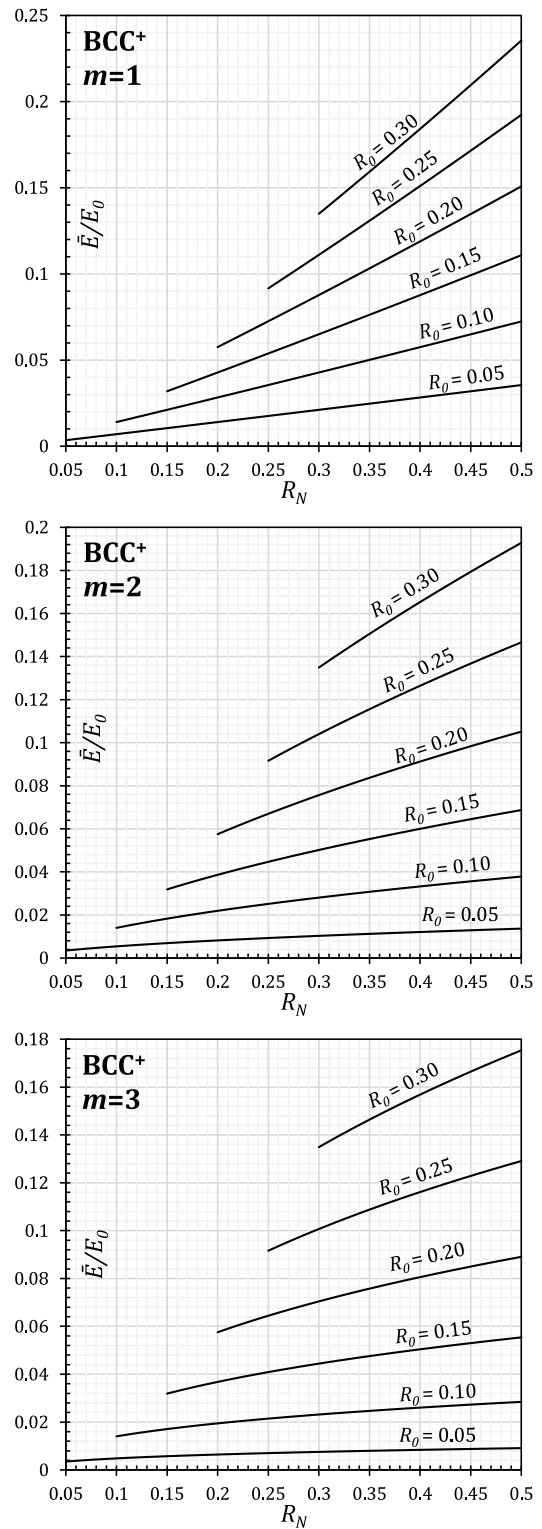

Fig. D.6. The relative effective elastic modulus of BCC⁺ lattices for the power $m = 1$, 2, and 3, and different values of R_0 and R_N.

Appendix E. The calibrated correction factor κ for the modified Gibson-Ashby model

Fig. E.1 depicts the calibrated correction factor, κ in Eq. (21), for the proposed modified Gibson-Ashby model relating the effective relative elastic modulus to the effective relative density of SC, BCC, and BCC⁺
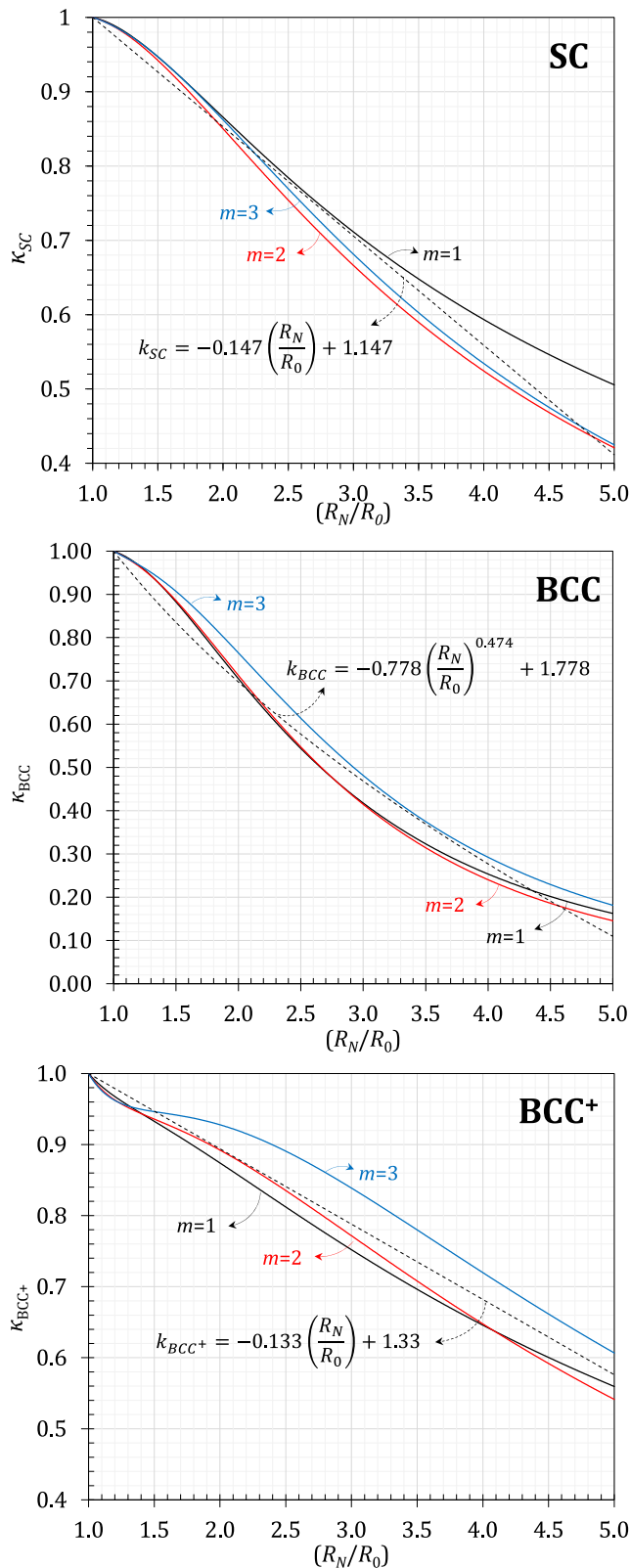
Fig. E.1. The calibrated κ parameter versus (R_N/R_0) for SC, BCC, and BCC⁺ graded lattices and the power $m = 1$, 2, and 3.

graded lattices, Eq. (20), and its local form, Eq. (23). Graphs are plotted for three different power of grading, $m = 1$, 2, and 3, and a wide range of the ratio, $1 < (R_N/R_0) < 5$ considering a high resolution of

$N = 100$. Note that for all the plots, the value of κ starts from one where $(R_N/R_0) = 1$ corresponds to a uniform lattice (standard Gibson-Ashby model in Eq. (19)).

References

Al-Saedi, Dheyaa S.J., Masood, S.H., 2018. Mechanical performance of functionally graded lattice structures made with selective laser melting 3D printing. In: IOP Conference Series: Materials Science and Engineering, Vol. 433. IOP Publishing, 012078. http://dx.doi.org/10.1088/1757-899X/433/1/012078.

Al-Saedi, Dheyaa S.J., Masood, S.H., Faizan-Ur-Rab, Muhammad, Alomarah, Amer, Ponnusamy, P., 2018. Mechanical properties and energy absorption capability of functionally graded F2BCC lattice fabricated by SLM. Mater. Des. 144, 32–44. http://dx.doi.org/10.1016/j.matdes.2018.01.059.

Bai, Long, Gong, Cheng, Chen, Xiaohong, Sun, Yuanxi, Xin, Liming, Pu, Huayan, Peng, Yan, Luo, Jun, 2020. Mechanical properties and energy absorption capabilities of functionally graded lattice structures: Experiments and simulations. Int. J. Mech. Sci. 182, 105735. http://dx.doi.org/10.1016/j.ijmecsci.2020.105735.

Cao, Xiaofei, Duan, Shengyu, Liang, Jun, Wen, Weibin, Fang, Daining, 2018. Mechanical properties of an improved 3D-printed rhombic dodecahedron stainless steel lattice structure of variable cross section. Int. J. Mech. Sci. 145, 53–63. http://dx.doi.org/10.1016/j.ijmecsci.2018.07.006.

Cao, Xiaofei, Jiang, Yongbo, Zhao, Tian, Wang, Panding, Wang, Yongzhen, Chen, Zihao, Li, Ying, Xiao, Dengbao, Fang, Daining, 2020. Compression experiment and numerical evaluation on mechanical responses of the lattice structures with stochastic geometric defects originated from additive-manufacturing. Composites B 194, 108030. http://dx.doi.org/10.1016/j.compositesb.2020.108030.

Cao, Xiaofei, Yang, Haoming, Ren, Xianben, Wu, Wenwang, Xi, Li, Li, Ying, Fang, Daining, 2021. Mechanical performance and defect analysis of the imperfect micro smooth gyroid cylinder shell structure. Compos. Struct. 273, 114320. http://dx.doi.org/10.1016/j.compstruct.2021.114320.

Choy, Sing Ying, Sun, Chen Nan, Leong, Kah Fai, Wei, Jun, 2017. Compressive properties of functionally graded lattice structures manufactured by selective laser melting. Mater. Des. 131, 112–120. http://dx.doi.org/10.1016/j.matdes.2017.06.006.

Christensen, R.M., 1986. Mechanics of low density materials. J. Mech. Phys. Solids 34 (6), 563–578. http://dx.doi.org/10.1016/0022-5096(86)90037-2.

Fleck, N.A., Deshpande, V.S., Ashby, M.F., 2010. Micro-architectured materials: Past, present and future. Proc. R. Soc. Lond. Ser. A Math. Phys. Eng. Sci. 466 (2121), 2495–2516. http://dx.doi.org/10.1098/rspa.2010.0215.

Gharehbaghi, Hussain, Sadeghzade, Mohammad, Farrokhabadi, Amin, 2022. Introducing the new lattice structure based on the representative element double octagonal bipyramid. Aerosp. Sci. Technol. 121, 107383. http://dx.doi.org/10.1016/j.ast.2022.107383.

Gibson, L.J., Ashby, M.F., 1982. Mechanics of three-dimensional cellular materials. Proc. R. Soc. Lond. Ser. A Math. Phys. Eng. Sci. 382 (1782), 43–59. http://dx.doi.org/10.1098/rspa.1982.0088.

Gibson, Lorna J., Ashby, Michael F., 2014. Cellular Solids: Structure and Properties, second ed. Cambridge University Press, pp. 1–510. http://dx.doi.org/10.1017/CBO9781139878326.

Goodall, Russell, 2013. Porous metals: Foams and sponges. In: Advances in Powder Metallurgy: Properties, Processing and Applications. Woodhead Publishing, pp. 273–307. http://dx.doi.org/10.1533/9780857098900.2.273.

Gorgin Karaji, Z., Jahanmard, F., Mirzaei, A.H., van der Wal, B., Amin Yavari, S., 2020. A multifunctional silk coating on additively manufactured porous titanium to prevent implant-associated infection and stimulate bone regeneration. Biomed. Mater. (Bristol, England) 15 (6), 065016. http://dx.doi.org/10.1088/1748-605X/aba40b.

Hedayati, R., Sadighi, M., Mohammadi-Aghdam, M., Zadpoor, A.A., 2016a. Effect of mass multiple counting on the elastic properties of open-cell regular porous biomaterials. Mater. Des. 89, 9–20. http://dx.doi.org/10.1016/j.matdes.2015.09.052.

Hedayati, R., Sadighi, M., Mohammadi-Aghdam, M., Zadpoor, A.A., 2016b. Mechanical properties of regular porous biomaterials made from truncated cube repeating unit cells: Analytical solutions and computational models. Mater. Sci. Eng. C 60, 163–183. http://dx.doi.org/10.1016/j.msec.2015.11.001.

Heshmati, M., Jalali, S.K., 2019. Effect of radially graded porosity on the free vibration behavior of circular and annular sandwich plates. Eur. J. Mech. A Solids 74, 417–430. http://dx.doi.org/10.1016/j.euromechsol.2018.12.009.

Jalali, S.K., Beigrezaee, M.J., Pugno, Nicola M., 2021. Is it always worthwhile to resolve the governing equations of plate theories for graded porosity along the thickness? Compos. Struct. 256, 112960. http://dx.doi.org/10.1016/j.compstruct.2020.112960.

Jalali, S.K., Beigrezaee, M.J., Pugno, Nicola M., 2022. Reporting a misunderstanding in relating the Young's modulus to functionally graded porosity. Compos. Struct. 281, 115007. http://dx.doi.org/10.1016/j.compstruct.2021.115007.

Jalali, S.K., Heshmati, M., 2020. Vibration analysis of tapered circular poroelastic plates with radially graded porosity using pseudo-spectral method. Mech. Mater. 140, 103240. http://dx.doi.org/10.1016/j.mechmat.2019.103240.

Janbaz, Shahram, McGuinness, Molly, Zadpoor, Amir A., 2018. Multimaterial control of instability in soft mechanical metamaterials. Phys. Rev. A 9 (6), 064013. http://dx.doi.org/10.1103/PhysRevApplied.9.064013.

Kumar, Suresh, Murthy Reddy, K.V.V.S., Kumar, Anil, Rohini Devi, G., 2013. Development and characterization of polymer-ceramic continuous fiber reinforced functionally graded composites for aerospace application. Aerosp. Sci. Technol. 26 (1), 185–191. http://dx.doi.org/10.1016/j.ast.2012.04.002.

Maconachie, Tobias, Leary, Martin, Lozanovski, Bill, Zhang, Xuezhe, Qian, Ma, Faruque, Omar, Brandt, Milan, 2019. SLM lattice structures: Properties, performance, applications and challenges. http://dx.doi.org/10.1016/j.matdes.2019.108137.

Mahbod, Mahshid, Asgari, Masoud, 2019. Elastic and plastic characterization of a new developed additively manufactured functionally graded porous lattice structure: Analytical and numerical models. Int. J. Mech. Sci. 155, 248–266. http://dx.doi.org/10.1016/j.ijmecsci.2019.02.041.

Mahmoud, Dalia, Elbestawi, Mohamed A., 2017. Lattice structures and functionally graded materials applications in additive manufacturing of orthopedic implants: A review. J. Manuf. Mater. Process. 1 (2), 13. http://dx.doi.org/10.3390/jmmp1020013.

Maskery, Ian, Hussey, Alexandra, Panesar, Ajit, Aremu, Adedeji, Tuck, Christopher, Ashcroft, Ian, Hague, Richard, 2017. An investigation into reinforced and functionally graded lattice structures. J. Cell. Plast. 53 (2), 151–165. http://dx.doi.org/10.1177/0021955X16639035.

McKown, S., Shen, Y., Brookes, W.K., Sutcliffe, C.J., Cantwell, W.J., Langdon, G.S., Nurick, G.N., Theobald, M.D., 2008. The quasi-static and blast loading response of lattice structures. Int. J. Impact Eng. 35 (8), 795–810. http://dx.doi.org/10.1016/j.ijimpeng.2007.10.005.

Menges, G., Knipschild, F., 1975. Estimation of mechanical properties for rigid polyurethane foams. Polym. Eng. Sci. 15 (8), 623–627. http://dx.doi.org/10.1002/pen.760150810.

Mora, Samantha, Pugno, Nicola M., Misseroni, Diego, 2022. 3D printed architected lattice structures by material jetting. Mater. Today http://dx.doi.org/10.1016/j.mattod.2022.05.008.

Parihar, Rityuj Singh, Setti, Srinivasu Gangi, Sahu, Raj Kumar, 2018. Recent advances in the manufacturing processes of functionally graded materials: A review. IEEE J. Sel. Top. Quantum Electron. 25 (2), 309–336. http://dx.doi.org/10.1515/secm-2015-0395.

Pompe, W., Worch, H., Epple, M., Friess, W., Gelinsky, M., Greil, P., Hempel, U., Scharnweber, D., Schulte, K., 2003. Functionally graded materials for biomedical applications. Mater. Sci. Eng. A 362 (1–2), 40–60. http://dx.doi.org/10.1016/S0921-5093(03)00580-X.

Popoola, Patricia A.I., Farotade, Gabriel, Fatoba, Olawale S., Popoola, Olawale, 2016. Laser engineering net shaping method in the area of development of functionally graded materials (FGMs) for aero engine applications - A review. In: Fiber Laser. InTech, http://dx.doi.org/10.5772/61711.

Ptochos, Evangelos, Labeas, George, 2012. Elastic modulus and Poisson's ratio determination of micro-lattice cellular structures by analytical, numerical and homogenisation methods. J. Sandw. Struct. Mater. 14 (5), 597–626. http://dx.doi.org/10.1177/1099636212444285.

Ram, S.C., Chattopadhyay, K., Chakrabarty, I., 2017. High temperature tensile properties of centrifugally cast in-situ Al-Mg2Si functionally graded composites for automotive cylinder block liners. J. Alloys Compd. 724, 84–97. http://dx.doi.org/10.1016/j.jallcom.2017.06.306.

Reddy, Ande Harshavardhan, Davuluri, Saritha, Boyina, Dhatreyi, 2020. 3D printed lattice structures: A brief review. In: Proceedings of the 2020 IEEE 10th International Conference on "Nanomaterials: Applications and Properties", NAP 2020. IEEE, pp. 02SAMA10–1–02SAMA10–5. http://dx.doi.org/10.1109/NAP51477.2020.9309680.

Roberts, A.P., Garboczi, E.J., 2001. Elastic moduli of model random three-dimensional closed-cell cellular solids. Acta Mater. 49 (2), 189–197. http://dx.doi.org/10.1016/S1359-6454(00)00314-1, arXiv:0009004.

Rodrigo, C., Xu, S., Durandet, Y., Ruan, D., 2021. Uniaxial compression of bi-directionally graded lattice structures: Finite element modelling. IOP Conf. Ser.: Mater. Sci. Eng. 1067 (1), 012107. http://dx.doi.org/10.1088/1757-899x/1067/1/012107.

Saleh, Bassiouny I., Ahmed, Mahmoud H., 2020. Development of functionally graded tubes based on pure Al/Al2O3 metal matrix composites manufactured by centrifugal casting for automotive applications. Met. Mater. Int. 26 (9), 1430–1440. http://dx.doi.org/10.1007/s12540-019-00391-3.

Saleh, Bassiouny, Jiang, Jinghua, Fathi, Reham, Al-hababi, Tareq, Xu, Qiong, Wang, Lisha, Song, Dan, Ma, Aibin, 2020. 30 Years of functionally graded materials: An overview of manufacturing methods, applications and future challenges. Composites B 201, 108376. http://dx.doi.org/10.1016/j.compositesb.2020.108376.

Ushijima, K., Cantwell, W.J., Mines, R.A.W., Tsopanos, S., Smith, M., 2011. An investigation into the compressive properties of stainless steel micro-lattice structures. J. Sandw. Struct. Mater. 13 (3), 303–329. http://dx.doi.org/10.1177/1099636210380997.

van Manen, Teunis, Janbaz, Shahram, Jansen, Kaspar M.B., Zadpoor, Amir A., 2021. 4D printing of reconfigurable metamaterials and devices. Commun. Mater. 2 (1), 56. http://dx.doi.org/10.1038/s43246-021-00165-8.

Wu, Helong, Yang, Jie, Kitipornchai, Sritawat, 2020. Mechanical analysis of functionally graded porous structures: A review. http://dx.doi.org/10.1142/S0219455420410151.

Yakout, Mostafa, Elbestawi, M.A., Veldhuis, Stephen C., 2019. Density and mechanical properties in selective laser melting of invar 36 and stainless steel 316L. J. Mater Process. Technol. 266, 397–420. http://dx.doi.org/10.1016/j.jmatprotec.2018.11.006.

Zadpoor, Amir A., 2019. Mechanical performance of additively manufactured meta-biomaterials. http://dx.doi.org/10.1016/j.actbio.2018.12.038.

Zadpoor, Amir Abbas, Hedayati, Reza, 2016. Analytical relationships for prediction of the mechanical properties of additively manufactured porous biomaterials. J. Biomed. Mater. Res. A 104 (12), 3164–3174. http://dx.doi.org/10.1002/jbm.a.35855.

Zargarian, Ali, Esfahanian, Mohsen, Kadkhodapour, Javad, Ziaei-Rad, Saeid, Zamani, Delaram, 2019. On the fatigue behavior of additive manufactured lattice structures. Theor. Appl. Fract. Mech. 100, 225–232. http://dx.doi.org/10.1016/j.tafmec.2019.01.012.

Zhang, X.Z., Leary, M., Tang, H.P., Song, T., Qian, M., 2018. Selective electron beam manufactured Ti-6Al-4V lattice structures for orthopedic implant applications: Current status and outstanding challenges. http://dx.doi.org/10.1016/j.cossms.2018.05.002.